http://www.aimspress.com/journal/mine

Mathematics in Engineering, 5(4): 1–44.
DOI:10.3934/mine.2023075
Received: 12 December 2022
Revised: 21 January 2023
Accepted: 23 January 2023
Published: 01 February 2023

Research article

Nanoparticle-based organic polymer retinal prostheses: modeling, solution map and simulation

Greta Chiaravalli[1,2], **Guglielmo Lanzani**[1,2], **Riccardo Sacco**[3,*] **and Sandro Salsa**[3]

[1] Center for Nanoscience and Technology, Istituto Italiano di Tecnologia, via Pascoli 70, 20133 Milano, Italy

[2] Dipartimento di Fisica, Politecnico di Milano, Piazza Leonardo da Vinci 32, 20133 Milano, Italy

[3] Dipartimento di Matematica, Politecnico di Milano, Piazza Leonardo da Vinci 32, 20133 Milano, Italy

* **Correspondence:** Email: riccardo.sacco@polimi.it; Tel: +390223994540.

Abstract: In this article we investigate a mathematical model for a retinal prosthesis made of organic polymer nanoparticles (NP) in the stationary regime. The model consists of a Drift-Diffusion system to describe free charge transport in the NP bulk; a Poisson-Nernst-Planck system to describe ion electrodiffusion in the solution surrounding the NP; and nonlinear transmission conditions at the NP-solution interface. To solve the model we use an iteration procedure for which we prove the existence and briefly comment the uniqueness of a fixed point under suitable smallness assumptions on model parameters. For system discretization we use a stabilized finite element method to prevent unphysical oscillations in the electric potential, carrier number densities and ion molar densities. Model predictions describe the amount of active chemical molecule accumulating at the neuron surface and highlight electrostatic effects induced by the sole presence of the nanoparticle. These results support the use of mathematical modeling as a virtual laboratory for the optimal design of bio-hybrid systems, whose investigation may be impervious due to experimental limits.

Keywords: multiscale and multiphysics modeling; nonlinear interface coupling; ion electrodiffusion; drift-diffusion charge transport; neuron depolarization; functional iterations

1. Introduction

Ocular pathologies represent a serious danger for the health and life quality of million individuals worldwide because in extreme manifestations they may turn out into loss of eyesight. This is the case, for instance, with Retinitis Pigmentosa (RP), a hereditary degeneration characterized by a progressive

dysfunction of rod and cone photoreceptors [31], and Age-related Macular Degeneration (AMD), a pathology of the macula, the small central area of the retina that controls vision acuity.

AMD is the main cause of blindness in subjects aged ≥55 years [7, 21]. Currently, 67 million people are affected by AMD in the EU [15] and 11 million individuals are affected with AMD in the U.S. [21], with a global prevalence of 170 million. The prevalence of AMD in the U.S. is anticipated to increase to 22 million by the year 2050, and the global prevalence is expected to increase to 288 million by the year 2040 [7,21]. Existing noninvasive approaches for the cure of RP and AMD, such as gene therapy, neuroprotection and pharmacology [19], can be effectively applied at early stages of the disease, otherwise more invasive therapeutic interventions, such as injection of anti-VEGF drugs [11] and/or photodynamic laser treatment [26], must be employed to treat late disease stages.

A valid alternative to the above mentioned medical cure for RP and AMD has been suggested in recent years by the development of biocompatible implantable prostheses [8,22,32]. Retinal prostheses have been shown to successfully stimulate the inner retinal network, but severe technical difficulties and undesired side effects have strongly limited so far their efficacy in the application on individuals. These limitations may have been overcome by the advent of a second generation of prosthetics based on conjugated polymers [2] which has been translated into a functioning technology in [20] and [6] where conjugated polymer nanoparticles (P3HT NPs) are subretinally injected in a rat model of RP and shown to mediate light-evoked stimulation of retinal neurons and persistently rescue visual functions.

Despite P3HT NPs open up a wide potential in the application of retinal prosthetics to the cure of pathologies secondary to photoreceptor death, the physical mechanisms underlying their function are still poorly understood. For this reason, in this article we conduct a theoretical and numerical study of a mathematical model, developed from that proposed in [4, 6], to describe the stationary function of a bio-hybrid system constituted by: (*i*) a P3HT NP; (*ii*) a retinal neuron; (*iii*) an aqueous extracellular region; and (*iv*) an interstitial cleft separating the NP from the retinal neuron. The theoretical model translates into mathematical relations the chain of physical events that transform an external supply of light stimulation into a depolarization of the retinal neuron upon mediation of the P3HT NP, and consists of the Drift-Diffusion (DD) system [12,30] to describe light photoconversion into free charged carriers in the NP bulk and the Poisson-Nernst-Planck (PNP) system [13, 14, 23, 27] to describe ion electrodiffusion in the aqueous medium.

We solve the model in one spatial dimension with the Gummel Map, a functional iteration customarily employed in inorganic semiconductor device simulation [10], for which we are able to prove the existence of a fixed point, upon introducing suitable smallness limitations on model parameters and coefficients. The Gummel Map reduces the nonlinear coupling between the DD system and the PNP system into a sequence of spatially heterogenous, linearized balance equations for electric potential (in both NP and aqueous medium), ion molar densities (in the sole aqueous medium) and photogenerated carrier number densities (in the sole NP). For each considered balance equation, interdomain connection is dealt with through transmission conditions expressing: (a) electron-driven molecular oxygen reduction at the NP-solution interface; (b) electrostatic coupling between NP and surrounding aqueous environment; and (c) ion electrodiffusion between extracellular bath and interstitial cleft.

The sequence of linearized boundary value problems is discretized using the finite element method with proper stabilization terms to prevent spurious unphysical oscillations in the electric potential and ensure positivity of the carrier number densities and ion molar densities in their respective domains of

definition [24, Chapters 22–23].

The above described computational model is then used to simulate the response of the bio-hybrid system to given input sources. Simulations provide a physical picture of the mechanisms occurring inside the NP when coupled with an electrolytic solution. In particular, model predictions seem to suggest that the coupling between the neuron and the NP may affect cleft polarization due to an electrostatic effect. Simulations also provide a quantitative estimate of the superoxide anion concentration that reaches the neuron membrane at different light intensities. This information may be biologically relevant because superoxide molecules may activate chemical pathways or induce oxidative distress at the neuron cellular membrane.

An outline of the article is as follows. In Section 2 we introduce the geometric scheme of the bio-hybrid system, the dependent variables of the problem and the scaling factors that are used to adimensionalize the equation system. In Section 3 we write the boundary value problems (in scaled form) which constitute the nonlinearly coupled differential model of the system. In Section 4 we describe the various steps of the Gummel Map that is used to iteratively solve the nonlinearly coupled model, while in Section 5 we describe the basic structure of the Gummel Map and state the theorem of existence of a fixed point of the proposed solution map also commenting on its uniqueness. The proof of the theorem is described in detail in Section 8. In Section 6 we illustrate the finite element approximation of the boundary value problems constituting the Gummel Map while in Section 7 we deal with the validation of the proposed model and algorithm and we illustrate the main results obtained from our numerical formulation. We close the article with Section 9, in which we draw the principal conclusions on the investigated bio-hybrid system and indicate future research directions.

2. Preliminaries

In Section 2.1 we describe the geometric representation of the bio-hybrid system under investigation. Then, in Section 2.2 we introduce the dependent variables of the problem (electric potential, ion molar densities and carrier number densities) together with their respective domain of definition. Finally, in Section 2.3 we define the scaling factors which are used to write the model equations in adimensional form.

2.1. Geometric representation of the bio-hybrid system

Figure 1 (left panel) shows a three-dimensional (3D) schematic representation of the bio-hybrid system studied in the present work. The system is composed of (*i*) the cytoplasm of a retinal neuron (indicated as "Neuron" in the left panel of Figure 1); (*ii*) the plasma membrane of the neuron (indicated as "Plasma Membrane" in the left panel of Figure 1); (*iii*) a P3HT NP (indicated as "NP" in the left panel of Figure 1); (*iv*) an aqueous extracellular region (indicated as "Extracellular Medium" in the left panel of Figure 1); and (*v*) a porous interstitial cleft separating the NP from the retinal neuron (indicated as "Interstitial Cleft" in the left panel of Figure 1). The yellow arrow represents the external input light source. The rotational invariance of the system with respect to the z axis allows us to reduce the 3D structure (in the cartesian reference system x-y-z) into the two-dimensional (2D) axial symmetric structure depicted in the middle panel of Figure 1 (x-z axisymmetric coordinate system). To further reduce model complexity, we introduce the one-dimensional (1D) open interval $\Omega = (0, L)$ represented in the right panel of Figure 1. The origin $x = 0$ is set in correspondence of the interface

between the cleft region and the neuron membrane. The cleft region is represented by the open interval $\Omega_1 = (0, R_1)$. The NP is represented by the open interval $\Omega_2 = (R_1, R_2)$. The extracellular region is represented by the open interval $\Omega_3 = (R_2, L)$. The computational domain for the nonlinear differential system is $\Omega = \Omega_1 \cup \Omega_2 \cup \Omega_3$. We also set $\Omega_{1,3} := \Omega_1 \cup \Omega_3$. The nonlinear conductance G_{NL} which connects the points $x = R_1$ and $x = R_2$ is a lumped electric representation of ion motion from the extracellular medium into the cleft in the 2D scheme in the middle panel of Figure 1.

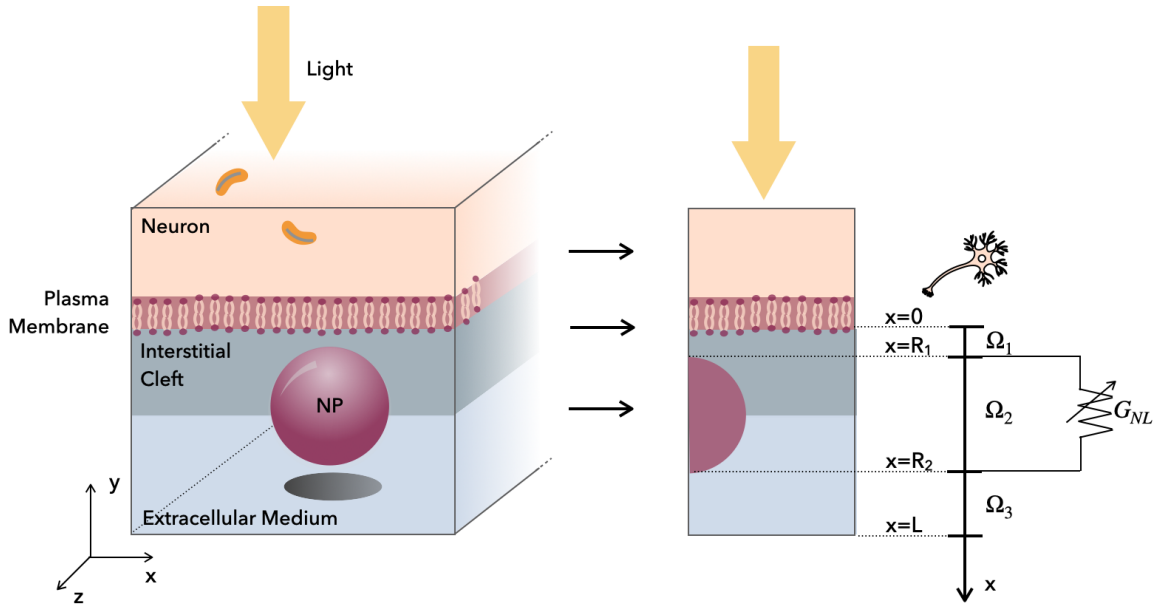

Figure 1. Left panel: three-dimensional view of the bio-hybrid system. Middle panel: two-dimensional axisymmetric scheme; Right panel: one-dimensional geometric reduction.

2.2. *Dependent variables*

To describe in mathematical terms the physical mechanisms occurring in each subdomain Ω_i, $i = 1, 2, 3$; at the interfaces $x = 0$, $x = R_1$, $x = R_2$ and $x = L$; and across the nonlinear conductance G_{NL}, we need:

- the electric potential ψ (units: V);
- the chemical variables n and p representing the carrier number densities of electrons and holes that are photogenerated in the NP (units: m^{-3});
- the chemical variables c_α, $\alpha = \{\mathrm{Na}^+, \mathrm{Cl}^-, \mathrm{K}^+\}$, representing the ion molar densities that passively flow in the cleft and extracellular regions (units: $\mathrm{mol\,m}^{-3} = \mathrm{mM}$), where Na^+, Cl^- and K^+ indicate sodium, chlorine and potassium, respectively;
- the chemical variable c representing the ion molar density of superoxide O_2^- (units: mM) that is generated at the interfaces $x = R_1$ and $x = R_2$ between NP and surrounding medium, and that subsequently flows by electrodiffusion in the extracellular medium and cleft.

We have:

$$\psi : \Omega \to \mathbb{R}, \tag{2.1a}$$

$$n,\ p : \Omega_2 \to \mathbb{R}^+, \tag{2.1b}$$

$$c_\alpha : \Omega_{1,3} \to \mathbb{R}^+, \tag{2.1c}$$

$$c : \Omega_{1,3} \to \mathbb{R}^+. \tag{2.1d}$$

From the above definitions we see that n, p, c_α and c are positive quantities. This property is a consequence of the Maxwell-Boltzmann statistics:

$$n = n_{ref} \exp\left(\frac{\psi - \varphi_n}{V_{th}}\right), \tag{2.2a}$$

$$p = n_{ref} \exp\left(\frac{\varphi_p - \psi}{V_{th}}\right), \tag{2.2b}$$

$$c_\alpha = c_{ref} \exp\left(z_\alpha \frac{\varphi_\alpha - \psi}{V_{th}}\right), \tag{2.2c}$$

$$c = c_{ref} \exp\left(\frac{\psi - \varphi}{V_{th}}\right), \tag{2.2d}$$

where φ_n, φ_p, φ_α and φ are the electrochemical potentials of electrons, holes and ions (units: V), V_{th} is the thermal voltage (units: V), n_{ref} is the reference number density (units: m^{-3}), c_{ref} is the reference molar density (units: mM) and z_α is the chemical valence of each ion, with $z_\alpha = +1$ for Na^+ and K^+ and $z_\alpha = -1$ for Cl^- and O_2^-.

For further elaboration, it is useful to introduce the following set of alternative depedent variables:

$$u_n = n_{ref} \exp\left(-\frac{\varphi_n}{V_{th}}\right), \tag{2.3a}$$

$$u_p = n_{ref} \exp\left(+\frac{\varphi_p}{V_{th}}\right), \tag{2.3b}$$

$$u_\alpha = c_{ref} \exp\left(z_\alpha \frac{\varphi_\alpha}{V_{th}}\right), \tag{2.3c}$$

$$u = c_{ref} \exp\left(-\frac{\varphi}{V_{th}}\right). \tag{2.3d}$$

The above dependent variables will be referred to henceforth as Slotboom variables in analogy with the Drift-Diffusion model for semiconductor devices (see [29]). From (2.3), we see that u_n, u_p, u_α and u are strictly positive quantities and

$$n = u_n \exp\left(+\frac{\psi}{V_{th}}\right), \tag{2.4a}$$

$$p = u_p \exp\left(-\frac{\psi}{V_{th}}\right), \tag{2.4b}$$

$$c_\alpha = u_\alpha \exp\left(-z_\alpha \frac{\psi}{V_{th}}\right), \tag{2.4c}$$

$$c = u \exp\left(\frac{\psi}{V_{th}}\right). \tag{2.4d}$$

2.3. Scaling

In the remainder of the article every quantity will be scaled by an appropriate positive constant referred to as "scaling factor". Precisely, let $\mathcal{U}$ denote a variable whose units are U. Assume that U^* is a quantity whose units are U. Then, the scaled variable associated with $\mathcal{U}$ is defined as

$$\widehat{\mathcal{U}} = \frac{\mathcal{U}}{U^*}. \tag{2.5}$$

Table 1 summarizes the expressions and the values of the scaling factors for the model variables and parameters. The symbol t represents the time coordinate.

Table 1. First column: variable; second column: scaling factor; third column: mathematical expression; fourth column: units; fifth column: numerical value of the scaling factor.

Variable	Scaling factor	Expression	Units	Value
x	x^*	L	m	$430 \cdot 10^{-9}$
ψ, g	ψ^*	V_{th}	V	$26.64 \cdot 10^{-3}$
φ_n, φ_p	ψ^*	V_{th}	V	$26.64 \cdot 10^{-3}$
φ_α, φ	ψ^*	V_{th}	V	$26.64 \cdot 10^{-3}$
n, p, u_n, u_p	n^*	n_{intr}	m^{-3}	10^{12}
c_α, u_α, u	c^*	c_{ref}	$\mathrm{mM} = \mathrm{mol\,m}^{-3}$	118
ρ_j, $j = 1, 3$	$\rho^*_{1,3}$	$c^* N_{Av}$	m^{-3}	$7.106 \cdot 10^{25}$
ρ_2	ρ^*_2	n^*	m^{-3}	10^{12}
C^0_m, C_m	C^*_m	ε_0 / x^*	$\mathrm{F\,m}^{-2}$	$2.059 \cdot 10^{-5}$
D_α, D	D^*	$\max\left\{D_\alpha,\, D,\, D_n,\, D_p\right\}$	$\mathrm{m}^2\,\mathrm{s}^{-1}$	$2.03 \cdot 10^{-9}$
D_n, D_p	D^*	$\max\left\{D_\alpha,\, D,\, D_n,\, D_p\right\}$	$\mathrm{m}^2\,\mathrm{s}^{-1}$	$2.03 \cdot 10^{-9}$
t, τ_n, τ_p	t^*	$(x^*)^2 / D^*$	s	$9.108 \cdot 10^{-5}$
G, $\mathcal{R}$	G^*	n^* / t^*	$\mathrm{m}^{-3}\,\mathrm{s}^{-1}$	$1.098 \cdot 10^{16}$
P_α, P	P^*	D^* / x^*	ms^{-1}	$4.721 \cdot 10^{-3}$
k_p	k^*_p	P^* / n^*	$\mathrm{m}^4\mathrm{s}^{-1}$	$4.721 \cdot 10^{-15}$
k_n	k^*_n	$k^*_p c^*$	$\mathrm{mol\,m\,s}^{-1}$	$5.571 \cdot 10^{-13}$

3. The mathematical model of the bio-hybrid system

In this section we illustrate the boundary value problems (in scaled form) that constitute the nonlinearly coupled differential formulation of the bio-hybrid system. For reader's ease we denote each scaled variable with the same symbol used to represent the variable in its dimensional form. Throughout the text we use $(\cdot)'$ as a shorthand notation for $\partial(\cdot)/\partial x$.

3.1. The boundary value problem for the electric potential

The electric potential ψ is governed by the nonlinear Poisson equation (NLP)

$$-\frac{\partial}{\partial x}\left(\varepsilon(x)\frac{\partial \psi}{\partial x}\right) = \lambda^{-2} f\left(x,\, \psi,\, u_\alpha,\, u,\, u_n,\, u_p\right) \quad \text{in } \Omega. \tag{3.1a}$$

The piecewise constant function ε is the dielectric permittivity defined as

$$\varepsilon(x) = \begin{cases} \varepsilon_1, & x \in \Omega_1, \\ \varepsilon_2, & x \in \Omega_2, \\ \varepsilon_3, & x \in \Omega_3, \end{cases} \tag{3.1b}$$

ε_j being the value of the relative dielectric permittivity in each subdomain Ω_j, $j = 1, 2, 3$. The function f is the space charge density defined as

$$f\left(x,\, \psi,\, u_\alpha,\, u,\, u_n,\, u_p\right) = \begin{cases} \gamma_1 \left(\displaystyle\sum_\alpha z_\alpha u_\alpha \exp\left(-z_\alpha \psi\right) - u \exp\psi + \rho_1 \right) & \text{in } \Omega_1 \\ \gamma_2 \left(u_p \exp\left(-\psi\right) - u_n \exp\psi + \rho_2 \right) & \text{in } \Omega_2 \\ \gamma_1 \left(\displaystyle\sum_\alpha z_\alpha u_\alpha \exp\left(-z_\alpha \psi\right) - u \exp\psi + \rho_3 \right) & \text{in } \Omega_3. \end{cases} \tag{3.1c}$$

The quantities ρ_j, $j = 1, 2, 3$, are given functions of x and physically represent the doping profile in each region Ω_j. The quantities γ_1 and γ_2 are dimensionless parameters defined as:

$$\gamma_1 = \frac{c^* N_{Av}}{N^*} \equiv \frac{n_{ref}}{N^*}, \tag{3.2}$$

$$\gamma_2 = \frac{n^*}{N^*} = \frac{n_{intr}}{N^*}, \tag{3.3}$$

$$N^* = \max\left\{n_{ref},\, n^*\right\}, \tag{3.4}$$

where $N_{Av} = 6.022 \cdot 10^{23}$ is the Avogadro's constant (units: mol^{-1}). Based on the values of c^* and n^* (see Table 1), it turns out that $N^* = n_{ref} = c^* N_{Av}$, so that $\gamma_1 = 1$ and $\gamma_2 = 1.407 \cdot 10^{-14}$.

Finally, the quantity λ has the following expression

$$\lambda = \frac{\lambda_D}{x^*}, \tag{3.5}$$

λ_D being the Debye length (units: m) defined as

$$\lambda_D = \sqrt{\frac{\varepsilon_0 \psi^*}{q N^*}}, \tag{3.6}$$

where $\varepsilon_0 = 8.854 \cdot 10^{-12}$ (units: $\mathrm{F\,m}^{-1}$) and $q = 1.602 \cdot 10^{-19}$ (units: C) are the dielectric permittivity of vacuum and the electron charge, respectively.

Remark 3.1. *The numerical value of λ_D is $1.4394 \cdot 10^{-10}$ m and the value of the dimensionless parameter λ^2 is $1.1205 \cdot 10^{-7}$. Since $\lambda^2 \ll 1$, the NLP equation* (3.1a) *has a markedly singularly perturbed nature. We refer to [18] for a detailed analysis of the singular perturbation property of the NLP equation in the case of inorganic semiconductor devices.*

The boundary conditions for (3.1a) are defined as follows.

$$-\varepsilon_1\psi'(0) + C_m^0\psi(0) = C_m^0\psi_N, \tag{3.7a}$$
$$\varepsilon_1\psi'(R_1^-) + C_m\psi(R_1^-) = C_m\psi(R_1^+), \tag{3.7b}$$
$$-\varepsilon_2\psi'(R_1^+) + C_m\psi(R_1^+) = C_m\psi(R_1^-), \tag{3.7c}$$
$$+\varepsilon_2\psi'(R_2^-) + C_m\psi(R_2^-) = C_m\psi(R_2^+), \tag{3.7d}$$
$$\varepsilon_3\psi'(R_2^+) + C_m\psi(R_2^+) = C_m\psi(R_2^-), \tag{3.7e}$$
$$\psi(1) = 0. \tag{3.7f}$$

The expressions (3.7a)–(3.7e) are linear transmission conditions that physically represent the capacitive coupling between neighbouring subdomains. C_m^0 and C_m denote the specific capacitance of the neuron membrane and of the NP surface, respectively, and ψ_N is the neuron resting potential. The expression (3.7f) is a Dirichlet boundary condition that fixes the electric potential to ground in correspondence of a position ($x = 1$) in the extracellular medium that is sufficiently far from the interface with the nanoparticle at $x = R_2$.

Remark 3.2. *The electric potential ψ is, in general, a discontinuous function over the domain Ω. In particular, according to the transmission conditions*(3.7a)–(3.7e)*, ψ has a jump at $x = 0$, $x = R_1$ and $x = R_2$. We see that if $C_m^0 \to +\infty$ and $C_m \to +\infty$, then the capacitive coupling is so strong that the electric potential becomes a continuous function over $\overline{\Omega}$. Conversely, if $C_m^0 \to 0^+$ and $C_m \to 0^+$, then the capacitive coupling is so weak that the nanoparticle subdomain Ω_2 becomes completely decoupled from Ω_1 and Ω_3. In this case, the electric potential turns out to be defined up to an arbitrary constant in both Ω_1 and Ω_2, and further compatibility conditions have to be enforced to determine the constant in both subdomains.*

3.2. The boundary value problems for the ions $u_\alpha, \alpha = Na^+, Cl^-, K^+$

The ion molar densities u_α, $\alpha = \{\mathrm{Na}^+, \mathrm{Cl}^-, \mathrm{K}^+\}$, are governed by the following continuity equation

$$-\frac{\partial}{\partial x}\left(D_\alpha(x)\exp(-z_\alpha\psi)\frac{\partial u_\alpha}{\partial x}\right) = 0 \qquad \text{in } \Omega_{1,3}, \tag{3.8a}$$

where

$$D_\alpha(x) = \begin{cases} D_\alpha^1 & x \in \Omega_1, \\ D_\alpha^3 & x \in \Omega_3. \end{cases} \tag{3.8b}$$

We introduce the following quantities:

$$S_\alpha(P, \psi(X), \psi(Y)) = P\,Be\left(z_\alpha(\psi(X) - \psi(Y))\right)e^{-z_\alpha\psi(Y)}, \tag{3.9}$$
$$Be(W) := \frac{W}{e^W - 1}. \tag{3.10}$$

The boundary conditions for the restriction of u_α in Ω_1 are:

$$-D_\alpha^1 e^{-z_\alpha\psi(0)}u_\alpha'(0) + S_\alpha(P_\alpha, \psi_N, \psi(0))u_\alpha(0) = S_\alpha(P_\alpha, \psi(0), \psi_N)u_{\alpha,N}, \tag{3.11a}$$

$$D^1_\alpha e^{-z_\alpha \psi(R_1^-)} u'_\alpha(R_1^-) + S_\alpha(P_{\alpha,i}, \psi(R_2^+), \psi(R_1^-)) u_\alpha(R_1^-) \tag{3.11b}$$
$$= S_\alpha(P_{\alpha,i}, \psi(R_1^-), \psi(R_2^+)) u_\alpha(R_2^+).$$

The boundary conditions for the restriction of u_α in Ω_3 are:

$$-D^3_\alpha e^{-z_\alpha \psi(R_2^+)} u'_\alpha(R_2^+) + S_\alpha(P_{\alpha,i}, \psi(R_1^-), \psi(R_2^+)) u_\alpha(R_2^+) \tag{3.11c}$$
$$= S_\alpha(P_{\alpha,i}, \psi(R_2^+), \psi(R_1^-)) u_\alpha(R_1^-),$$
$$u_\alpha(1) = \overline{u}_\alpha. \tag{3.11d}$$

For the purpose of analysis, it is convenient to perform in Ω_3 the following change of dependent variable

$$v_\alpha := u_\alpha - \overline{u}_\alpha. \tag{3.11e}$$

Inserting (3.11e) into (3.8a) yields

$$-\left(D^3_\alpha e^{-z_\alpha \psi} v'_\alpha\right)' = 0 \qquad \text{in } \Omega_3. \tag{3.11f}$$

The boundary conditions for v_α are:

$$-D^3_\alpha e^{-z_\alpha \psi(R_2^+)} v'_\alpha(R_2^+) + S_\alpha(P_{\alpha,i}, \psi(R_1^-), \psi(R_2^+))(v_\alpha(R_2^+) + \overline{u}_\alpha) \tag{3.11g}$$
$$= S_\alpha(P_{\alpha,i}, \psi(R_2^+), \psi(R_1^-))(v_\alpha(R_1^-) + \overline{u}_\alpha),$$
$$v_\alpha(1) = 0. \tag{3.11h}$$

The quantity $u_{\alpha,N}$ is a positive constant denoting the value of the ion molar density u_α in the neuron. The quantity $\overline{u}_\alpha$ is a positive constant denoting the value of the ion molar density u_α in the extracellular medium, far from $x = R_2$. The quantities P_α denote the permeability to ion u_α of the neuron membrane. The quantities $P_{\alpha,i}$ denote the permeability to ion u_α of the nonlinear conductance G_{NL} which represents with a lumped equivalent electric parameter the electrodiffusive flow of ions between cleft Ω_1 and extracellular region Ω_3.

The expressions (3.11a)–(3.11c) are transmission conditions that physically represent the electrodiffusive coupling between neighbouring subdomains according to the Goldman-Hodgkin-Katz model [24, Chapter 17]. The expression (3.11d) is a Dirichlet boundary condition that fixes the ion molar density to the equilibrium value in correspondence of a position ($x = 1$) in the extracellular medium that is sufficiently far from the interface with the nanoparticle at $x = R_2$.

3.3. The boundary value problem for the superoxide ion $u = u_{O_2^-}$

The superoxide ion molar density $u = u_{O_2^-}$ is governed by the following continuity equation

$$-\frac{\partial}{\partial x}\left(D(x) e^{\psi} \frac{\partial u}{\partial x}\right) + \frac{k_1 \tilde{C}\, e^{\psi}}{C^{EQ}} u = k_1 \tilde{C} \quad \text{in } \Omega_{1,3}, \tag{3.12a}$$

where

$$D(x) = \begin{cases} D_1 & x \in \Omega_1 \\ D_3 & x \in \Omega_3. \end{cases} \tag{3.12b}$$

The quantity k_1 is the rate of the kinetic reaction (3.22). The quantity C^{EQ} is the superoxide ion equilibrium molar density of the kinetic reaction (3.22). The quantity $\tilde{C}$ is the molar density of molecular oxygen O_2 dissolved into the aqueous solution in which the NP is immersed.

We introduce the following quantities:

$$\mathcal{S}(\psi(X),\, \psi(Y), u_p(Y)) = k_p e^{\left[\psi(X)-\psi(Y)\right]} u_p\,(Y)\,, \tag{3.13}$$

$$\mathcal{W}\,(\psi(X),\, \psi(Y),\, u(Y),\, u_n(X)) = k_n e^{\psi(X)-g(\psi(Y),u(Y))} u_n(X). \tag{3.14}$$

The boundary conditions for the restriction of u in Ω_1 are:

$$u'\,(0) = 0, \tag{3.15a}$$

$$\begin{aligned} &D_1 e^{\psi\left(R_1^-\right)} u'\,\left(R_1^-\right) + \mathcal{S}(\psi(R_1^-),\, \psi(R_1^+), u_p(R_1^+)) u\,\left(R_1^-\right) \\ &= \mathcal{W}\,\left(\psi(R_1^+),\, \psi(R_1^-),\, u(R_1^-),\, u_n(R_1^+)\right). \end{aligned} \tag{3.15b}$$

The boundary conditions for the restriction of u in Ω_3 are:

$$\begin{aligned} &- D_3 e^{\psi\left(R_2^+\right)} u'\,\left(R_2^+\right) + \mathcal{S}(\psi(R_2^+),\, \psi(R_2^-), u_p(R_2^-)) u\,\left(R_2^+\right) \\ &= \mathcal{W}\,\left(\psi(R_2^-),\, \psi(R_2^+),\, u(R_2^+),\, u_n(R_2^-)\right), \end{aligned} \tag{3.15c}$$

$$u'\,(1) = 0. \tag{3.15d}$$

The expressions (3.15a) and (3.15d) are homogeneous Neumann boundary conditions which physically represent the fact that no superoxide ion flux density can flow out of the computational domain. The expressions (3.15b) and (3.15c) are nonlinear Robin boundary conditions which physically represent the net balance between the recombination and generation processes that regulate consumption and production of O_2^- at the interfaces between the NP and the surrounding environment.

3.4. The boundary value problems for the photogenerated carriers

The photogenerated carriers u_n and u_p are governed by the following continuity equations:

$$-\frac{\partial}{\partial x}\left(D_n e^{\psi}\frac{\partial u_n}{\partial x}\right) = \eta G - \mathcal{R}(u_p, u_n, \psi) \qquad \text{in } \Omega_2, \tag{3.16a}$$

$$-\frac{\partial}{\partial x}\left(D_p e^{-\psi}\frac{\partial u_p}{\partial x}\right) = \eta G - \mathcal{R}(u_p, u_n, \psi) \qquad \text{in } \Omega_2. \tag{3.16b}$$

The quantity G is a given function of x and represents the light illumination rate. The dimensionless quantity η is the photogeneration efficiency. The function $\mathcal{R}$ is defined as

$$\mathcal{R}(u_p, u_n, \psi) = \frac{u_p u_n - 1}{\tau_p(u_n e^{\psi} + 1) + \tau_n(u_p e^{-\psi} + 1)}, \tag{3.16c}$$

and physically represents the net recombination rate due to two-particle interaction, according to the Shockley-Read-Hall theory [28], τ_n and τ_p being the electron and hole lifetimes, respectively. At thermodynamic equilibrium conditions (corresponding to switching illumination off, $G = 0$), $u_n u_p = 1$ so that $\mathcal{R} = 0$ and both u_n and u_p are constant. If $u_n u_p > 1$, then $\mathcal{R} > 0$ and both u_n and u_p tend to

decrease due to the fact that recombination prevails over generation. Conversely, if $u_n u_p < 1$, then $\mathcal{R} < 0$ and both u_n and u_p tend to increase due to the fact that generation prevails over recombination.

We introduce the following quantities:

$$Q_n(\psi(X),\, \psi(Y),\, u(Y)) = k_n \frac{n_{ref}}{n_{intr}} e^{\psi(X) - g(\psi(Y),\, u(Y))}, \tag{3.17}$$

$$Q_p(\psi(X),\, \psi(Y),\, u(X)) = k_p \frac{n_{ref}}{n_{intr}} e^{\psi(X) - \psi(Y)} u(X). \tag{3.18}$$

The boundary conditions for u_n are:

$$D_n e^{\psi(R_1^+)} u_n'(R_1^+) = Q_n(\psi(R_1^+),\, \psi(R_1^-),\, u(R_1^-)) u_n(R_1^+), \tag{3.19a}$$

$$-D_n e^{\psi(R_2^-)} u_n'(R_2^-) = Q_n(\psi(R_2^-),\, \psi(R_2^+),\, u(R_2^+)) u_n(R_2^-). \tag{3.19b}$$

The boundary conditions for u_p are:

$$D_p e^{\psi(R_1^+)} u_p'(R_1^+) = Q_p(\psi(R_1^-),\, \psi(R_1^+),\, u(R_1^-)) u_p(R_1^+), \tag{3.19c}$$

$$-D_p e^{\psi(R_2^-)} u_p'(R_2^-) = Q_p(\psi(R_2^+),\, \psi(R_2^-),\, u(R_2^+)) u_p(R_2^-). \tag{3.19d}$$

The expressions (3.19a)–(3.19b) are nonlinear Robin boundary conditions that physically represent the surface mechanisms of conversion of photogenerated electrons into superoxide ions according to the Marcus-Gerischer theory [17]. The expressions (3.19c)–(3.19d) are Robin boundary conditions that physically represent the surface mechanisms of recombination of photogenerated holes with the superoxide ions that are present at $x = R_1$ and $x = R_2$. The quantities k_n and k_p are the tunneling coefficient for electrons in the P3HT and the hole surface recombination probability, respectively. The function g is defined as follows

$$g = g(x) = g(\psi(x), u(x)) = \begin{cases} \dfrac{(A + \psi(x) + \ln u(x))^2}{B} & \text{if } u(x) \le \tilde{C}, \\ \dfrac{(A + \psi(x) + \ln \tilde{C})^2}{B} & \text{if } u(x) > \tilde{C}, \end{cases} \tag{3.20}$$

where A and B are constants, $B > 0$, and $\tilde{C}$ is a positive constant such that

$$0 < C^{EQ} < \tilde{C} \ll 1, \tag{3.21}$$

C^{EQ} denoting the superoxide ion equilibrium molar density of the kinetic reaction which transforms molecular oxygen O_2 into superoxide O_2^-

$$O_2 + e \to O_2^-. \tag{3.22}$$

4. The Gummel Map: solution algorithm

In this section we illustrate the Gummel Map for the decoupled solution of the nonlinear differential model constituted by the boundary value problems (3.1), (3.8), (3.12) and (3.16). The solution algorithm is inspired by the fixed-point iteration originally introduced in [10] and customarily adopted in the simulation of inorganic semiconductor devices with the DD model (see [12, 18]).

For a given tolerance $\delta > 0$ and given $u_\alpha^{(k)}$, $u^{(k)}$, $u_n^{(k)}$ and $u_p^{(k)}$, $k \ge 0$, the fixed-point iteration proposed in this work consists of the successive execution of the following steps:

S.1 solve the nonlinear Poisson (NLP) equation for the electric potential:

$$-\frac{\partial}{\partial x}\left(\varepsilon(x)\frac{\partial\psi^{(k+1)}}{\partial x}\right)=\lambda^{-2}f\left(x,\,\psi^{(k+1)},\,u_\alpha^{(k)},\,u^{(k)},\,u_n^{(k)},\,u_p^{(k)}\right)\quad\text{in }\Omega, \tag{4.1a}$$

with the following boundary conditions:

$$-\varepsilon_1\left(\psi^{(k+1)}\right)'(0)+C_m^0\psi^{(k+1)}(0)=C_m^0\psi_N, \tag{4.1b}$$
$$\varepsilon_1\left(\psi^{(k+1)}\right)'(R_1^-)+C_m\psi^{(k+1)}(R_1^-)=C_m\psi^{(k+1)}(R_1^+), \tag{4.1c}$$
$$-\varepsilon_2\left(\psi^{(k+1)}\right)'(R_1^+)+C_m\psi^{(k+1)}(R_1^+)=C_m\psi^{(k+1)}(R_1^-), \tag{4.1d}$$
$$+\varepsilon_2\left(\psi^{(k+1)}\right)'(R_2^-)+C_m\psi^{(k+1)}(R_2^-)=C_m\psi^{(k+1)}(R_2^+), \tag{4.1e}$$
$$\varepsilon_3\left(\psi^{(k+1)}\right)'(R_2^+)+C_m\psi^{(k+1)}(R_2^+)=C_m\psi^{(k+1)}(R_2^-). \tag{4.1f}$$
$$\psi^{(k+1)}(1)=0; \tag{4.1g}$$

S.2 solve the linearized continuity equation for the ion molar density of Na^+, Cl^- and K^+:

$$-\frac{\partial}{\partial x}\left(D_\alpha(x)\exp\left(-z_\alpha\psi^{(k+1)}(x)\right)\frac{\partial u_\alpha^{(k+1)}}{\partial x}\right)=0\qquad\text{in }\Omega_1\cup\Omega_3, \tag{4.2a}$$

with the following boundary conditions:

$$-D_\alpha^1 e^{-z_\alpha\psi^{(k+1)}(0)}\left(u_\alpha^{(k+1)}\right)'(0)+S_\alpha(P_\alpha,\psi_N,\psi^{(k+1)}(0))u_\alpha^{(k+1)}(0)=S_\alpha(P_\alpha,\psi^{(k+1)}(0),\psi_N)u_{\alpha,N}, \tag{4.2b}$$
$$D_\alpha^1 e^{-z_\alpha\psi^{(k+1)}(R_1^-)}\left(u_\alpha^{(k+1)}\right)'(R_1^-)+S_\alpha(P_{\alpha,i},\psi^{(k+1)}(R_2^+),\psi^{(k+1)}(R_1^-))u_\alpha^{(k+1)}(R_1^-) \tag{4.2c}$$
$$=S_\alpha(P_{\alpha,i},\psi^{(k+1)}(R_1^-),\psi^{(k+1)}(R_2^+))u_\alpha^{(k+1)}(R_2^+),$$
$$-D_\alpha^3 e^{-z_\alpha\psi(R_2^+)}\left(u_\alpha^{(k+1)}\right)'(R_2^+)+S_\alpha(P_{\alpha,i},\psi^{(k+1)}(R_1^-),\psi^{(k+1)}(R_2^+))u_\alpha^{(k+1)}(R_2^+) \tag{4.2d}$$
$$=S_\alpha(P_{\alpha,i},\psi^{(k+1)}(R_2^+),\psi^{(k+1)}(R_1^-))u_\alpha^{(k+1)}(R_1^-),$$
$$u_\alpha^{(k+1)}(1)=\overline{u}_\alpha; \tag{4.2e}$$

S.3 solve the linearized continuity equation for the ion molar density of O_2^-:

$$-\frac{\partial}{\partial x}\left(D(x)e^{\psi^{(k+1)}(x)}\frac{\partial u^{(k+1)}(x)}{\partial x}\right)+\frac{k_1\tilde{C}\,e^{\psi^{(k+1)}(x)}}{C^{EQ}}u^{(k+1)}(x)=k_1\tilde{C}\quad\text{in }\Omega_1\cup\Omega_3, \tag{4.3a}$$

(4.3b)

with the following boundary conditions:

$$\left(u^{(k+1)}\right)'(0)=0, \tag{4.3c}$$
$$D_1 e^{\psi^{(k+1)}(R_1^-)}\left(u^{(k+1)}\right)'(R_1^-)+\mathcal{S}(\psi^{(k+1)}(R_1^-),\,\psi^{(k+1)}(R_1^+),u_p^{(k)}(R_1^+))u^{(k+1)}(R_1^-) \tag{4.3d}$$
$$=\mathcal{W}\left(\psi^{(k+1)}(R_1^+),\,\psi^{(k+1)}(R_1^-),\,u^{(k)}(R_1^-),\,u_n^{(k)}(R_1^+)\right),$$

$$- D_3 e^{\psi^{(k+1)}(R_2^+)} \left(u^{(k+1)}\right)'(R_2^+) + \mathcal{S}(\psi^{(k+1)}(R_2^+),\, \psi^{(k+1)}(R_2^-),\, u_p^{(k)}(R_2^-))u^{(k+1)}(R_2^+) \tag{4.3e}$$
$$= \mathcal{W}\left(\psi^{(k+1)}(R_2^-),\, \psi^{(k+1)}(R_2^+),\, u^{(k)}(R_2^+),\, u_n^{(k)}(R_2^-)\right),$$
$$\left(u^{(k+1)}\right)'(1) = 0; \tag{4.3f}$$

S.4 solve the linearized continuity equation for the photogenerated electrons:

$$-\frac{\partial}{\partial x}\left(D_n e^{\psi^{(k+1)}} \frac{\partial u_n^{(k+1)}}{\partial x}\right) = \eta G - \mathcal{R}_n(u_p^{(k)},\, u_n^{(k)},\, u_n^{(k+1)},\, \psi^{(k+1)}) \quad \text{in } \Omega_2\ , \tag{4.4a}$$

where

$$\mathcal{R}_n(u_p^{(k)},\, u_n^{(k)},\, u_n^{(k+1)},\, \psi^{(k+1)}) = \frac{u_p^{(k)} u_n^{(k+1)} - 1}{\tau_p(u_n^{(k)} e^{\psi^{(k+1)}} + 1) + \tau_n(u_p^{(k)} e^{-\psi^{(k+1)}} + 1)}, \tag{4.4b}$$

with the following boundary conditions:

$$D_n e^{\psi^{(k+1)}(R_1^+)} \left(u_n^{(k+1)}\right)'(R_1^+) = Q_n(\psi^{(k+1)}(R_1^+),\, \psi^{(k+1)}(R_1^-),\, u^{(k+1)}(R_1^-))u_n^{(k+1)}(R_1^+)\,, \tag{4.4c}$$
$$- D_n e^{\psi^{(k+1)}(R_2^-)} \left(u_n^{(k+1)}\right)'(R_2^-) = Q_n(\psi^{(k+1)}(R_2^-),\, \psi^{(k+1)}(R_2^+),\, u^{(k+1)}(R_2^+))u_n^{(k+1)}(R_2^-)\,; \tag{4.4d}$$

S.5 solve the linearized continuity equation for the photogenerated holes:

$$-\frac{\partial}{\partial x}\left(D_p e^{-\psi^{(k+1)}} \frac{\partial u_p^{(k+1)}}{\partial x}\right) = \eta G - \mathcal{R}_p(u_p^{(k)},\, u_n^{(k)},\, u_p^{(k+1)},\, \psi^{(k+1)}) \quad \text{in } \Omega_2, \tag{4.5a}$$

where

$$\mathcal{R}_p(u_p^{(k)},\, u_n^{(k)},\, u_p^{(k+1)},\, \psi^{(k+1)}) = \frac{u_p^{(k+1)} u_n^{(k)} - 1}{\tau_p(u_n^{(k)} e^{\psi^{(k+1)}} + 1) + \tau_n(u_p^{(k)} e^{-\psi^{(k+1)}} + 1)}, \tag{4.5b}$$

with the following boundary conditions:

$$D_p e^{\psi^{(k+1)}(R_1^+)} \left(u_p^{(k+1)}\right)'(R_1^+) = Q_p(\psi^{(k+1)}(R_1^-),\, \psi^{(k+1)}(R_1^+),\, u^{(k+1)}(R_1^-))u_p^{(k+1)}(R_1^+)\,, \tag{4.5c}$$
$$- D_p e^{\psi^{(k+1)}(R_2^-)} \left(u_p^{(k+1)}\right)'(R_2^-) = Q_p(\psi^{(k+1)}(R_2^+),\, \psi^{(k+1)}(R_2^-),\, u^{(k+1)}(R_2^+))u_p^{(k+1)}(R_2^-)\,; \tag{4.5d}$$

S.6 compute the maximum absolute relative increment of the electron electrochemical potential

$$\delta_n = \frac{\left\| -\ln\left(\dfrac{u_n^{(k+1)}}{u_n^{(k)}}\right)\right\|_\infty}{\left\| -\ln\left(u_n^{(k+1)}\right)\right\|_\infty} \qquad \text{in } \Omega_2; \tag{4.6}$$

S.7 compute the maximum absolute relative increment of the hole electrochemical potential

$$\delta_p = \frac{\left\| \ln\left(\dfrac{u_p^{(k+1)}}{u_p^{(k)}}\right)\right\|_\infty}{\left\| \ln\left(u_p^{(k+1)}\right)\right\|_\infty} \qquad \text{in } \Omega_2; \tag{4.7}$$

S.8 compute the maximum absolute relative increment of the electrochemical potentials of the Na^+, Cl^- and K^+ ions:

$$\delta_\alpha = \frac{\left\| \frac{1}{z_\alpha} \ln\left(\frac{u_\alpha^{(k+1)}}{u_\alpha^{(k)}}\right) \right\|_\infty}{\left\| \frac{1}{z_\alpha} \ln\left(u_\alpha^{(k+1)}\right) \right\|_\infty} \qquad \text{in } \Omega_1 \cup \Omega_3; \tag{4.8}$$

S.9 update the electrochemical potential of the O_2^- ion:

$$\delta_u = \frac{\left\| -\ln\left(\frac{u^{(k+1)}}{u^{(k)}}\right) \right\|_\infty}{\left\| -\ln\left(u^{(k+1)}\right) \right\|_\infty} \qquad \text{in } \Omega_1 \cup \Omega_3; \tag{4.9}$$

S.10 compute the maximum absolute relative increment:

$$\delta^{(k+1)} = \max\left(\delta_n, \delta_p, \delta_\alpha, \delta_u\right); \tag{4.10}$$

S.11 check for convergence:
if $\delta^{(k+1)} < \delta$ then terminate the iteration, otherwise go back to step 1. and continue.

A flow-chart of the sequence of the above steps is illustrated in Figure 2.

Remark 4.1. *From the algorithmic point of view, the solution map schematically represented in the flow-chart of Figure 2 consists of:*

- *the nonlinear step* **S.1** *to solve the NLP equation. This step, performed by using the Newton Method, is described in 4.1 and gives rise to the successive solution of a sequence of linear diffusion-reaction equations, with a positive reaction term, to update the electric potential;*
- *the sequence of linear steps* **S.2**–**S.5** *to solve the continuity equation for ions and carriers. Each step is a self-adjoint diffusion-reaction-production equation with nonnegative reaction and production terms.*

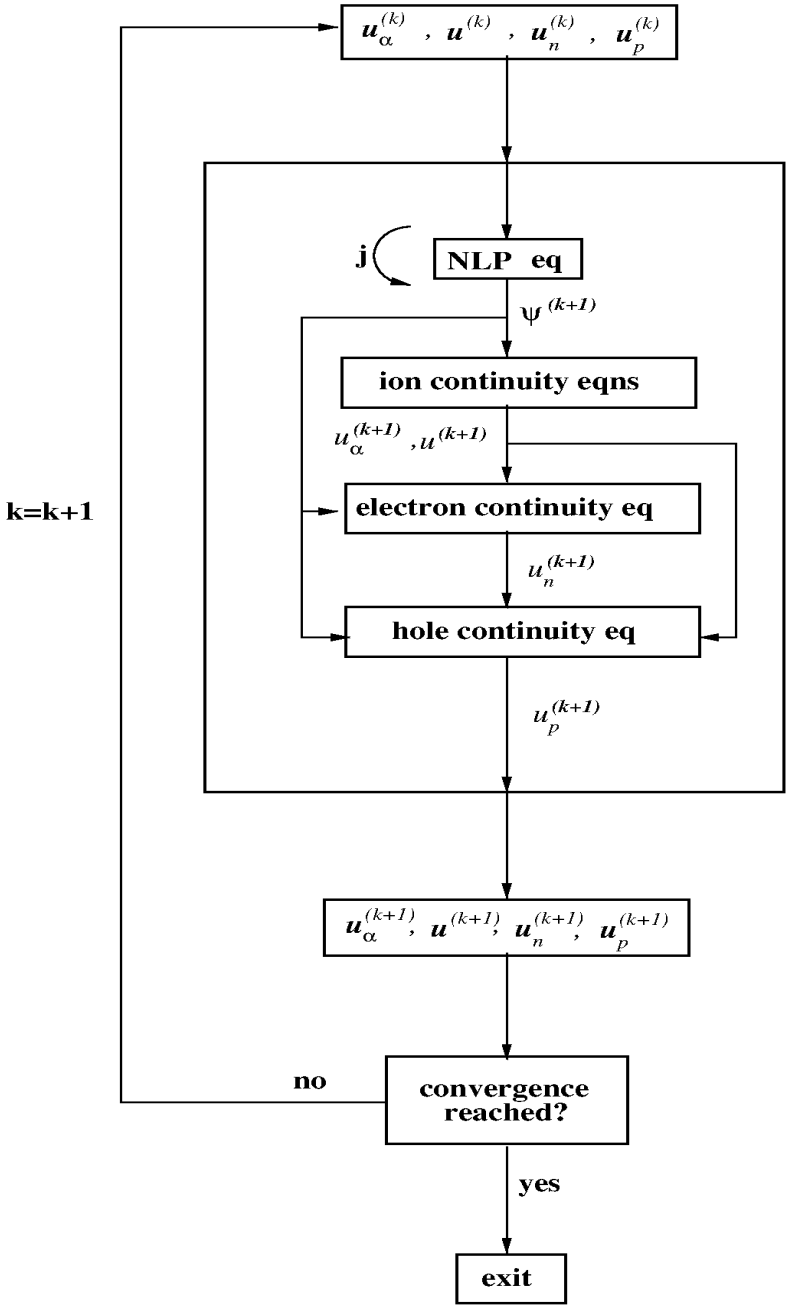

Figure 2. Flow-chart of the Gummel Map. The scheme shows which are the input variables and the output variables of each block. The arrow on the left-hand side of the NLP equation block refers to the iterative solution of the NLP equation using the Newton Method. The quantity j is the counter of the Newton iteration. The NLP eq box corresponds to Step S.1, the ion continuity eqns box to Steps S.2 and S.3, the electron continuity eq to Step S.4, the hole continuity eq to Step S.5 and the convergence box is related to Steps S.6–S.11.

4.1. Iterative solution of the NLP equation

The NLP equation (4.1a) can be written in the following residual form

$$\mathcal{N}_\psi(\psi^{(k+1)}) = 0 \qquad \text{in } \Omega, \tag{4.11a}$$

where

$$\mathcal{N}_\psi(\Phi) = -\frac{\partial}{\partial x}\left(\varepsilon(x)\frac{\partial \Phi}{\partial x}\right) - \lambda^{-2} f\left(x,\, \Phi,\, u_\alpha^{(k)},\, u^{(k)},\, u_n^{(k)},\, u_p^{(k)}\right) \tag{4.11b}$$

is the residual associated with the nonlinear operator $\mathcal{N}_\psi$. To iteratively solve (4.11a) through a linearization procedure, we use the Newton Method and denote by $j \geq 0$ the iteration counter. To initialize the Newton iteration we set $\psi^{(j=0)} = \psi^{(k)}$, where $\psi^{(k)}$ is the electric potential distribution currently available from the Gummel Map. Then, each j-th iteration of the Newton Method consists of the following two steps:

NM.1 compute the Newton increment $\delta\psi^{(j)}$ by solving

$$\mathcal{N}'_\psi(\psi^{(j)})\delta\psi^{(j)} = -\mathcal{N}_\psi(\psi^{(j)}) \qquad \text{in } \Omega, \tag{4.11c}$$

where

$$\mathcal{N}'_\psi(v)(\cdot) = -\frac{\partial}{\partial x}\left(\varepsilon(x)\frac{(\cdot)}{\partial x}\right) - \lambda^{-2}\frac{\partial f}{\partial \psi}\left(x,\, v,\, u_\alpha^{(k)},\, u^{(k)},\, u_n^{(k)},\, u_p^{(k)}\right)(\cdot) \tag{4.11d}$$

is the Frèchet derivative of the nonlinear operator $\mathcal{N}_\psi$ evaluated at v;

NM.1 update the Newton iterate through the relation

$$\psi^{(j+1)} = \psi^{(j)} + \delta\psi^{(j)}, \tag{4.11e}$$

until convergence is reached.

Let $j^* \geq 0$ denote the value of the iteration counter j in correspondence of which the sequence of steps **NM.1**–**NM.2** has reached convergence. The final step of the procedure for the solution of the NLP equation consists of setting

$$\psi^{(k+1)} = \psi^{(j^*)}. \tag{4.11f}$$

Then, we are in the position to continue the Gummel Map from step **S.2**.

5. The Gummel Map

In this section, we illustrate the structure of the solution map which is proposed to iteratively solve the fully nonlinear differential model described in Section 3. Then, we introduce an appropriate functional setting for the action of the fixed-point iteration, analyzing existence and uniqueness of a fixed-point.

5.1. Abstract formulation

We denote by $\mathbf{U} = \left(u_n, u_p, u_\alpha, u\right)$ the vector of photogenerated carrier number densities and ion molar densities. Then, we introduce the fixed-point operator

$$\mathbb{G} = \mathcal{P} \circ \mathcal{T}, \tag{5.1a}$$

where, for every $k \geq 0$,

$$\mathcal{T} : \mathbf{U}^{(k)} \to \psi^{(k+1)}, \tag{5.1b}$$

represents the nonlinear step **S.1** of Section 4 and

$$\mathcal{P} : \left(\psi^{(k+1)}, \mathbf{U}^{(k)}\right) \to \mathbf{U}^{(k+1)}, \tag{5.1c}$$

represents the sequence of linear steps **S.2**–**S.5** of Section 4.

Given $\mathbf{U}^{(0)}$, the Gummel Map described in Section 4 can be written in the form of a fixed-point iteration as

$$\mathbf{U}^{(k+1)} = \mathbb{G}(\mathbf{U}^{(k)}) \qquad \forall k \geq 0. \tag{5.1d}$$

The block structure of the Gummel Map (5.1d) is represented in the scheme of Figure 3.

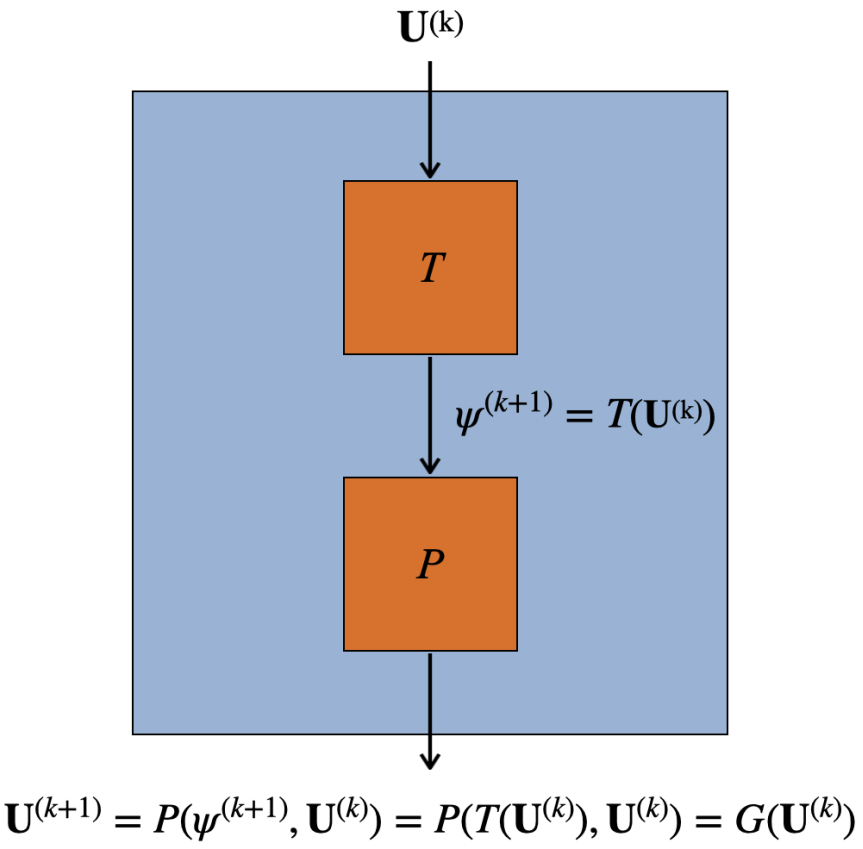

Figure 3. Block structure of the Gummel Map. Each iteration of the Gummel Map is the composition of a map $\mathcal{T}$ which updates the electric potential and a map $\mathcal{P}$ which updates the ion molar densities and the carrier number densities.

5.2. Functional setting

For any interval $\mathcal{S}$, in the following we denote $L^p(\mathcal{S})$, $p \in [1, \infty]$, the space of functions that are p-integrable over $\mathcal{S}$ and by $H^k(\mathcal{S})$, $k \geq 0$, the Sobolev space of functions that are square integrable over $\mathcal{S}$ with their first k derivatives (see [16] for an extensive discussion of Sobolev spaces and their properties). We also denote by $H^1_{0,\{1\}}(\Omega_3)$ the subset of $H^1(\Omega_3)$ of functions vanishing at $x = 1$ and we define:

$$u_\alpha(x) := 0,\ u(x) := 0 \qquad x \in \Omega_2, \tag{5.2a}$$

$$u_n(x) := 0,\ u_p(x) := 0 \qquad x \in \Omega_{1,3}. \tag{5.2b}$$

Relations (5.2) allow us to define the dependent variables u_α, u, u_n and u_p over *all* the computational domain $\Omega = \Omega_1 \cup \Omega_2 \cup \Omega_3$. In view of the subsequent theoretical analysis of the model, we introduce the broken H^1 spaces:

$$\mathcal{H}^1(\Omega) = \left\{ v : \Omega \to \mathbb{R} \ :\ v|_{\Omega_j} \in H^1\left(\Omega_j\right),\ j = 1, 2, 3 \right\}, \tag{5.3}$$

$$\mathcal{H}^1_{0,\{1\}}(\Omega) = \left\{ v \in \mathcal{H}^1(\Omega) \ :\ v(1) = 0 \right\}. \tag{5.4}$$

Then, we introduce the following function spaces (for the electric potential)

$$V = \left\{ v \in L^2(\Omega) \ :\ v \in \mathcal{H}^1_{0,\{1\}}(\Omega) \right\}, \tag{5.5a}$$

$$\mathcal{V} = \{ v \in V \ :\ -M_1 \leq v(x) \leq M_1 \ \ x \in \Omega \}, \tag{5.5b}$$

where

$$M_1 = \frac{C_I \max\{1, C_L\}}{\min\left\{\varepsilon_j, C^0_m, C_m\right\}}(K_1 + K_2 + K_3), \tag{5.5c}$$

and having introduced the positive constants C_I and C_L, and the following quantities:

$$K_1 = C^0_m \left|\psi_N\right| + \lambda^{-2}\gamma_1 \left\|\rho\right\|_{L^\infty(\Omega_{1,3})} \tag{5.5d}$$

$$+ \lambda^{-2}\gamma_2 \left\|\rho_2\right\|_{L^\infty(\Omega_2)} + 2\lambda^{-2}\gamma_1 \left\| \sum_{\alpha \neq O^-_2} z_\alpha u^{(0)}_\alpha \right\|_{L^\infty(\Omega_{1,3})}$$

$$K_2 = \lambda^{-2}\gamma_2 (R_2 - R_1) \left\| u^{(0)}_n - u^{(0)}_p \right\|_{L^\infty(\Omega_2)} \tag{5.5e}$$

$$K_3 = \lambda^{-2}\gamma_1 \left\| u^{(0)} \right\|_{L^1(\Omega_{1,3})}. \tag{5.5f}$$

We also introduce the following function spaces (for ions, electrons and holes), each one being a closed, bounded and convex set of $L^2(\Omega)$:

$$X_\alpha = \left\{ \phi_\alpha \in L^2(\Omega) \ :\ \phi_\alpha \in \mathcal{H}^1(\Omega),\ 0 \leq \phi_\alpha(x) \leq \mathcal{M}_\alpha,\ \ x \in \Omega \right\}, \tag{5.6a}$$

$$X_u = \left\{ \phi_u \in L^2(\Omega) \ :\ \phi_u \in \mathcal{H}^1(\Omega),\ 0 \leq \phi_u(x) \leq \mathcal{M}_u,\ \ x \in \Omega \right\}, \tag{5.6b}$$

$$X_{n,p} = \left\{ \phi_{n,p} \in L^2(\Omega) \ :\ \phi_{n,p} \in \mathcal{H}^1(\Omega),\ 0 \leq \phi_{n,p}(x) \leq N,\ \ x \in \Omega \right\}. \tag{5.6c}$$

Consistent with (5.2), we have:

$$\phi_\alpha(x) = \phi_u(x) = 0 \qquad x \in \Omega_2,$$
$$\phi_n(x) = \phi_p(x) = 0 \qquad x \in \Omega_{1,3}.$$

We set $N = G_{max}\tau_{max}$, where $G_{max} = \max_{x\in\Omega_2} G(x)$ and $\tau_{max} = \max\left\{\tau_{diff,n},\, \tau_{diff,p}\right\}$, $\tau_{diff,n}$ and $\tau_{diff,p}$ being the diffusion times of electrons and holes, respectively. We define:

$$\mathcal{M}_\alpha := \max\left\{u_{\alpha,N}, \bar{u}_\alpha\right\} \qquad \alpha = \left\{\mathrm{Na}^+,\, \mathrm{Cl}^-,\, \mathrm{K}^+\right\}, \tag{5.7}$$

$$\mathcal{M}_u := \frac{C_I e^M}{C_\delta}\left\{N\, k_n e^M + k_1\tilde{C}\right\}, \tag{5.8}$$

where:

$$M = \frac{\max\{1, C_L\}\, C_I}{\min\left\{\varepsilon_j, C_m^0, C_m\right\}}(C_m^0\,|\psi_N| + \lambda^{-2}\left\|f^0\,(x,0)\right\|_{L^2(\Omega)}), \tag{5.9}$$

$$C_\delta = \min\left\{D_1,\, D_3,\, \frac{k_1\tilde{C}}{C^{EQ}}\right\}. \tag{5.10}$$

Finally, to gather the nonreacting ions, the superoxide ion and the photogenerated carriers, we define the function space

$$\mathbf{X} \equiv (X_\alpha)^3 \times X_u \times (X_{n,p})^2. \tag{5.11}$$

Remark 5.1. *It is worth noting that $u_\alpha(x) > 0$ and $u(x) > 0$ for $x \in \overline{\Omega}_{1,3}$, while $u_{n,p}(x) > 0$ for $x \in \overline{\Omega}_2$. The reason why we have used the mathematical expression $0 \leq$, instead of $0 <$, in the definition of the spaces* (5.6) *is because of* (5.2).

5.3. Existence (and uniqueness) of a fixed point

The following theorem is the principal theoretical result of this article. For its proof, we refer to Section 8.

Theorem 5.1. *The Gummel Map* (5.1a) *has the following properties:*

a) $\mathbb{G} : \mathbf{X} \to \mathbf{X}$.

b) $\mathbb{G}$ *is continuous and compact.*

Then $\mathbb{G}$ *has a fixed point* $\mathbf{U}^* = \left(u_\alpha^*,\, u^*,\, u_p^*,\, u_n^*\right) \in \mathbf{X}$.
The electric potential associated with the fixed-point is $\psi^* = \mathcal{T}(\mathbf{U}^*)$ *such that* $\psi^* \in \mathcal{V}$, $\mathcal{T}$ *being the map defined in* (5.1b).

Corollary 5.2. *Setting*

$$\mathcal{M} := \max\left\{\mathcal{M}_\alpha,\, \mathcal{M}_u,\, N\right\}, \tag{5.12a}$$

we see that $\mathbb{G}$ *is endowed with the following invariant region*

$$\mathbf{Q} = Q^6, \tag{5.12b}$$

$$Q = \left\{q \in L^2(\Omega)\ :\ q \in \mathcal{H}^1(\Omega),\, 0 < q(x) \leq \mathcal{M},\ x \in \Omega\right\}. \tag{5.12c}$$

Remark 5.2. *For the meaning of invariant region, cf. [12].*

Remark 5.3. *As it is common in these kinds of models (e.g., semiconductor devices), uniqueness of a solution is not expected in general. In the present case, uniqueness of a fixed point for the Gummel Map can be restored by modifying in a rather straightforward way the estimates in the proof of Theorem 5.1, under additional restrictions on the parameters in* (5.5c) *and* $\mathcal{M}_\alpha$, $\mathcal{M}_u$ *in* (5.6a) *and* (5.6b)*, in order to make the Gummel Map a strict contraction.*

Remark 5.4. *Theorem 5.1 shows that the ion molar densities and the photogenerated carrier number densities are strictly positive in their domains of definition. This property agrees with physical expectation.*

6. Finite element approximation

This section is devoted to illustrate the numerical approximation of each linearized equation in the Gummel Map using the Galerkin Finite Element Method. To this purpose, it is immediate to verify that each linearized equation can be written in the general form of a diffusion-production-consumption equation for the dependent variable $\chi = \chi(x)$

$$\frac{\partial}{\partial x}\left(-a(x)\frac{\partial \chi(x)}{\partial x}\right) + s(x)\chi(x) = p(x) \qquad x \in \omega, \tag{6.1a}$$

where ω is an interval such that $\omega \subseteq \Omega$. The quantity $a = a(x)$ is the diffusion coefficient, such that

$$0 < a_{min} \leq a(x) \leq a_{max} \qquad \forall x \in \omega. \tag{6.1b}$$

The quantity $s = s(x)$ is the consumption coefficient, such that

$$0 \leq s(x) \leq s_{max} \qquad \forall x \in \omega. \tag{6.1c}$$

The quantity $p = p(x)$ is the production coefficient, whose sign is not predictable in the case of Eq (4.11c), whereas, in the case of the other equations in the Gummel Map, p is such that

$$0 \leq p(x) \leq p_{max} \qquad \forall x \in \omega. \tag{6.1d}$$

It is worth noticing that the diffusion coefficient $a = a(x)$ may be an exponential function of the electric potential. Therefore, a may experience significant variations, especially close to the boundary of ω where interface phenomena take place. The same consideration holds for the consumption and production coefficients, s and p. In such conditions, it is important to adopt a stable discretization scheme to prevent from spurious oscillations to arise in the numerical solution of (6.1a). Denoting by $\mathcal{T}_h$ a partition of ω into subintervals K (elements) of size h, the approach taken in the present article is based on the following choices:

- piecewise linear continuous finite elements;
- harmonic average of a over each $K \in \mathcal{T}_h$ (see [25]);
- mass lumping of the tridiagonal matrix corresponding to the consumption term;
- trapezoidal quadrature rule to evaluate the right-hand side of the linear system associated with the discrete form of (6.1a).

The benefits emanating from the above discretization strategy are:

- discretization error $e_h := \chi - \chi_h$ of order h and h^2 in the $H^1(\omega)$ and $L^2(\omega)$ norms, respectively;
- absence of unphysical oscillations in the spatial distributions of all the dependent variables over the interval ω;
- nonnegative spatial distributions of ion molar densities and photogenerated carrier number densities;
- weak conservation of the computed electric displacement vector, molar flux density of ions and carrier current densities over $\mathcal{T}_h$.

We refer to [24, Chapter 23] for more details on the theoretical and computational properties of the above described discretization strategy of the diffusion-production-consumption equation (6.1a).

7. Simulations

In this section we perform a series of simulation tests conducted by running a user-coded MatLab software which implements the algorithm illustrated in Section 4 and the finite element discretization scheme illustrated in Section 6. In Section 7.1 we analyze the convergence performance of the algorithm and verify the a priori bounds illustrated in Section 5. In Section 7.2 we investigate the role of each considered biophysical mechanism in the function of the bio-hybrid system studied in this article.

7.1. Convergence of Gummel's Map and a priori estimates

In Figure 4 (left panel) we represent the convergence history of the solution algorithm. On the x-axis, the quantity k, with $k \geq 0$, represents the number of Gummel's Map iterations and on the y-axis the quantity $\delta^{(k+1)}$ represents the maximum absolute relative increment on the electrochemical potentials computed using Eq (4.10). As customary in Numerical Analysis, $\delta^{(k+1)}$ is used as an estimator of the *actual* maximum absolute relative error. In the computations the tolerance δ was set equal to 10^{-5}. Interestingly, the plotted curve shows that the error decreases fastly during the first $\simeq$25 iterations, and then starts decreasing more slowly and non monotonically. In Figure 4 (right panel) we represent the number of NLP iterations $j = j(k)$ needed to meet a tolerance equal to 10^{-10} on the absolute maximum relative error of the Newton increment at each Gummel's Map iteration k. Results show that $j(k) \leq 4$ and $j(k) = 2$ for $k \geq 100$.

In Figure 5 (left panel) we represent the minimum and maximum values ψ_{min} and ψ_{max} of the electric potential ψ as a function of k. Results show that $\psi_{max} = 0$, corresponding to the Dirichlet datum at $x = 1$, where the electrolyte is supposed to be electroneutral, and $\psi_{min} = -0.6$, in the vicinity of the neuron membrane (see Section 7.2). In Figure 5 (right panel) we represent the minimum and maximum values $U_{p,min}$ and $U_{p,max}$ of the hole number density (blue color) and the minimum and maximum values $U_{n,min}$ and $U_{n,max}$ of the electron number density (red color) as a function of k. It is interesting to notice that in the case of holes $U_{p,min}$ and $U_{p,max}$ are almost overlapped, whereas in the case of electrons $U_{n,min}$ and $U_{n,max}$ differ by almost two orders of magnitude. These results are consistent with the physical transport properties of the two charge carriers: while the holes are able to redistribute across the domain Ω_2 due to their "elevated" mobility, the electrons are instead almost immobile, and spatially distribute themselves throughout Ω_2 according to the Lambert-Beer profile of

the light source G.

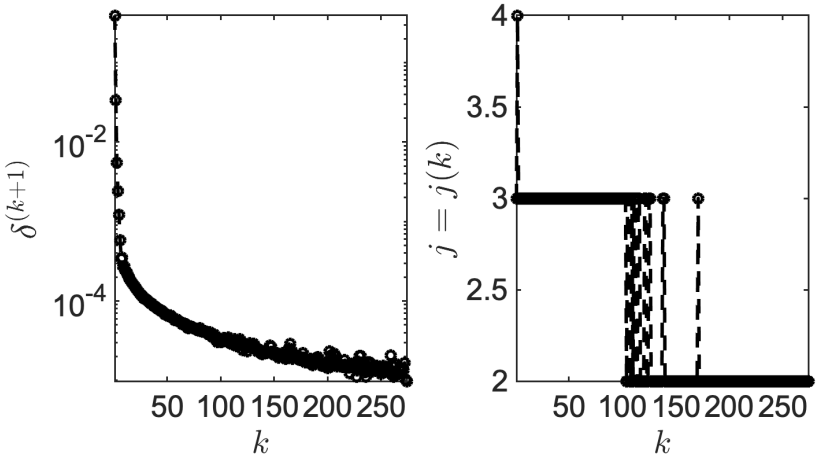

Figure 4. Left panel: plot of the maximum absolute relative error $\delta^{(k+1)}$ as a function of Gummel's Map iterations k. Right panel: plot of the number of NLP iterations $j = j(k)$ performed at each Gummel's Map iteration k.

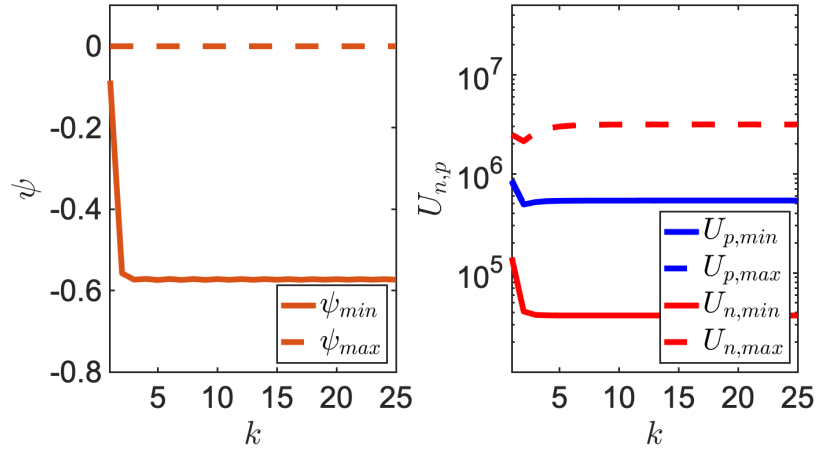

Figure 5. Left panel: plot of the minimum and maximum values of the electric potential ψ as a function of k. Right panel: plot of the minimum and maximum values of the hole number density U_p and of the minimum and maximum values of the electron number density U_n as a function of k.

In Figure 6 we represent the minimum and maximum values of the ion molar densities as a function of k in the subdomain Ω_1. It is interesting to notice that the behaviour of the O_2^- ion is markedly different from that of Na^+, Cl^- and K^+: both minimum and maximum values of O_2^- molar density increase monotonically to their corresponding limit values, whereas the minimum and maximum values of the other ions slowly converge with oscillations to their corresponding limit values.

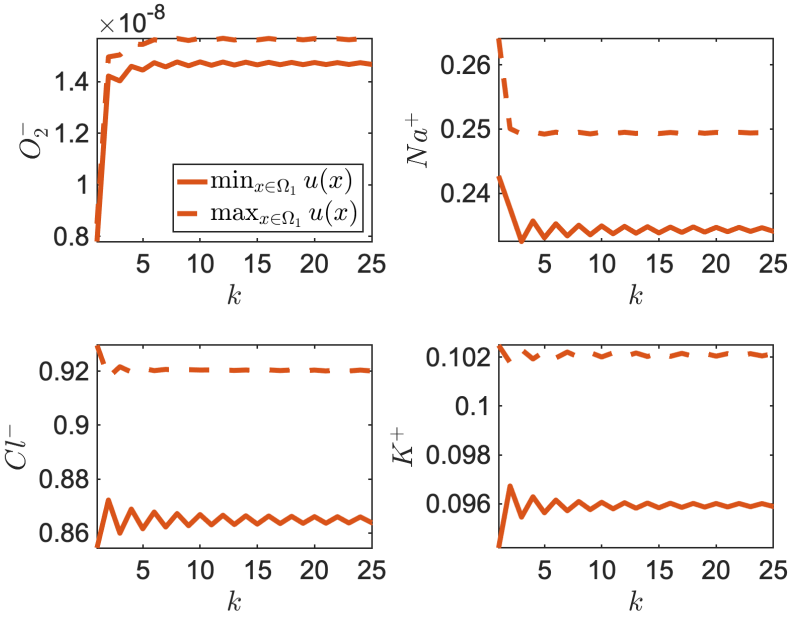

Figure 6. Plot of the minimum and maximum values of the molar density of O_2^- (top left panel), Na^+ (top right panel), Cl^- (bottom left panel) and K^+ (bottom right panel) in Ω_1, as a function of k.

7.2. Physical analysis of model predictions

Throughout the section we abandon the dimensionless form of the variables and represent each quantity with its units. This allows us to provide a consistent physical interpretation to the simulation results.

Table 2 provides a list of all the numerical values of model parameters used in the simulations. In Figure 7 we represent the piecewise spatial distribution of the electric potential over the computational domain $\Omega = (0, L)$, distinguishing the cleft region Ω_1 (left panel), the NP region Ω_2 (middle panel) and the electrolyte region Ω_3 (right panel). Results indicate that in the proximity of the neuron the electric potential exhibits a steep boundary layer due to the capacitive coupling induced by the cellular membrane on the cleft region. Inside the NP the electric potential has a linear behavior. In the electrolyte side the electric potential is clamped to the boundary value of 0 V enforced at $x = L$ which represents the electroneutrality of the biological electrolytic solution far away from the NP-neuron interface. In Figure 8 we show a zoom of the boundary layer of the electric potential ψ at the interface with the neuron in three different simulation conditions: (i) when no NP is present in the environment and the neuronal membrane is directly in contact with the bulk electrolyte (blue line); (ii) when the NP is present and forms a cleft region but it is not photo-activated by light; (iii) when the NP is present and is also activated by light. Results indicate that in case (i), the amplitude of the boundary layer is of $\simeq -1.5$ mV. In both cases (ii) and (iii), the qualitative behavior of the electric potential profile is the same as in case (i), but the amplitude of the electrostatic shift is of $\simeq -15$ mV. This physical behavior is to be solely ascribed to the interface electrostatic coupling of neuron and NP with the cleft electrolytic solution, expressed by Eqs (3.7b), (3.7d) and (3.7e). Other electrostatic coupling effects, such as that induced by the polarization of the nanoparticle or by the electrostatic production

and accumulation of superoxide anions in the cleft region are hindered by the presence of bulk ions in the cleft region, which are able to screen any polarizing effect in a few Debye lengths.

Table 2. Numerical values of model parameters used in the simulations. Left column: symbol representing the parameter; middle column: units; right column: numerical value of the parameter.

Parameter	Units	Value
L	m	$430 \cdot 10^{-9}$
R_1	m	$30 \cdot 10^{-9}$
R_2	m	$180 \cdot 10^{-9}$
C_m^0	$\mathrm{F\,m^{-2}}$	$9 \cdot 10^{-3}$
C_m	$\mathrm{F\,m^{-2}}$	7.45
$D_{O_2^-}$	$\mathrm{m^2\,s^{-1}}$	$2.1 \cdot 10^{-10}$
D_{Na^+}	$\mathrm{m^2\,s^{-1}}$	$1.33 \cdot 10^{-9}$
D_{Cl^-}	$\mathrm{m^2\,s^{-1}}$	$2.03 \cdot 10^{-9}$
D_{K^+}	$\mathrm{m^2\,s^{-1}}$	$1.96 \cdot 10^{-9}$
P_{Na^+}	$\mathrm{m\,s^{-1}}$	$6 \cdot 10^{-11}$
P_{Cl^-}	$\mathrm{m\,s^{-1}}$	$1 \cdot 10^{-9}$
P_{K^+}	$\mathrm{m\,s^{-1}}$	$4 \cdot 10^{-10}$
μ_n	$\mathrm{m^2\,V^{-1}s^{-1}}$	$1 \cdot 10^{-12}$
μ_p	$\mathrm{m^2\,V^{-1}s^{-1}}$	$1 \cdot 10^{-8}$
η	–	$5 \cdot 10^{-4}$
ε_1	–	6
ε_2	–	3.5
ε_3	–	80
k_n	$\mathrm{mol\,m\,s^{-1}}$	$9 \cdot 10^{-31}$
k_p	$\mathrm{m^4\,s^{-1}}$	$1 \cdot 10^{-30}$

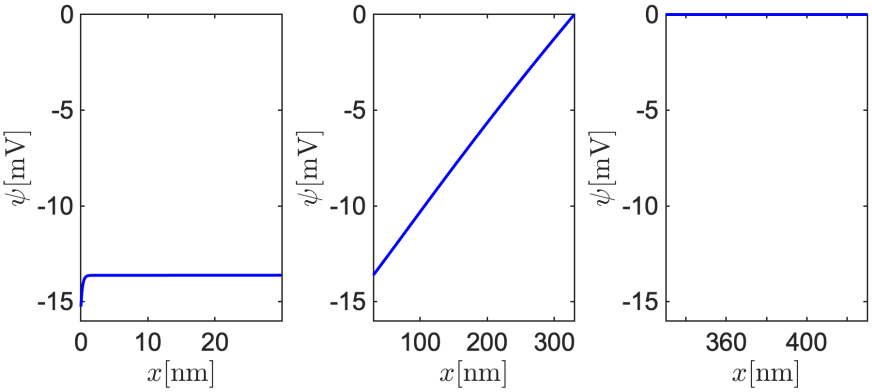

Figure 7. Piecewise electric potential profile simulated in the three regions of the computational domain Ω. Left panel: cleft, $\Omega_1 = (0, R_1)$; middle panel: NP, $\Omega_2 = (R_1, R_2)$; right panel: electrolytic solution, $\Omega_3 = (R_2, L)$.

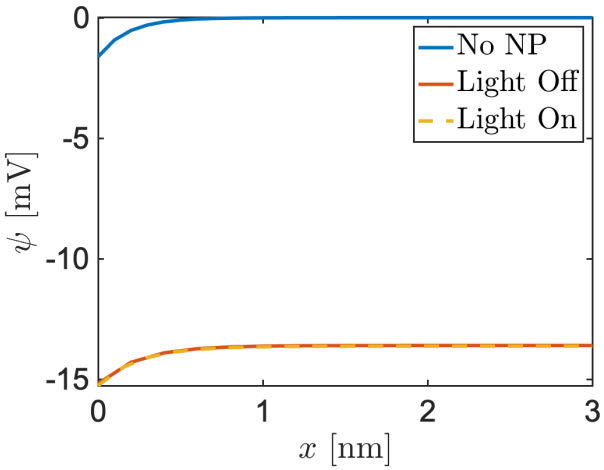

Figure 8. Zoom of the electric potential ψ at a distance of 3 nm from the neuron interface in three different simulation conditions. Blue line: no NP is present and the neuron is in contact with the bulk electrolyte. Orange line: the NP is present, but light is not polarizing it. Yellow line: the NP is illuminated.

In Figure 9 we represent the spatial distribution in the NP region Ω_2 of the number density of holes and electrons (p and n) and of their corresponding Slotboom variables (u_p and u_n). It is interesting to notice that holes are able to redistribute almost homogeneously across the NP domain (Figure 9 left) thanks to their high mobility. Electrons instead, due to the formation of $P3HT^+ : {}^3O_2^-$ with the molecular oxygen [3], are characterized by a mobility which is 4 orders of magnitude smaller than hole mobility, and, as a consequence, their spatial distribution closely resembles the Lambert-Beer profile of the input light G (Figure 9 right), in agreement with the considerations already drawn in Section 7.1 and in [4]. The strong asymmetry in the mobilities of the two charge carriers leads to the formation of a dipole-like distribution of positive and negative charge across the NP domain, which is responsible of the NP polarization. The combination of the asymmetric transport properties of holes and electrons inside P3HT with the asymmetric Lambert-Beer light profile, is an instance of the so-called Dember Effect [5, 9]. This effect leads to the formation of a dipole-like electric potential distribution, referred to as Dember photovoltage, and is caused by an asymmetric distribution of charge inside a semiconducting material due to a markedly different accumulation and redistribution of charges according to their transport properties and light incidence.

In Figure 10 we represent the spatial distribution of the ion molar density of the electrolytic ions across the whole domain Ω. Consistent with definitions (5.2a), all the ion molar densities are set equal to zero in Ω_2 since no ions are allowed to travel across the NP, a physical evidence of the high hydrophobicity of P3HT. Results indicate that O_2^- molar density increases with respect to its bulk concentration in the cleft region, where it gets accumulated (top left panel). In the simulation, light comes from the left, from the neuron towards the NP, inducing, as clearly visible in Figure 9, an accumulation of electrons at the NP-cleft interface. This favors the production of O_2^- compared to the bulk electrolyte side. It is also interesting to notice that a steep boundary layer shows up at the cellular membrane, due to the negative peak of the electric potential (see Figure 7, left panel). In the bulk electrolyte the O_2^- molar density, as well as that of the other bulk electrolytic ions, does not depart significantly from its Dirichlet boundary value at $x = L$. Bulk ions, such as Na^+, Cl^- and K^+, show in

the cleft a different behaviour depending on their valence and their Nernst potential in contact with the neuron. In particular, Cl^- and Na^+, whose concentration is low in the intracellular region, are reduced with respect to their bulk concentrations, whereas K^+ is accumulating. Depending on the valence of each ion, the formed boundary layer exhibits a different slope: cations tend to accumulate around a peak of negative potential, whereas anions tend to deplete the boundary layer in proximity of the cell membrane.

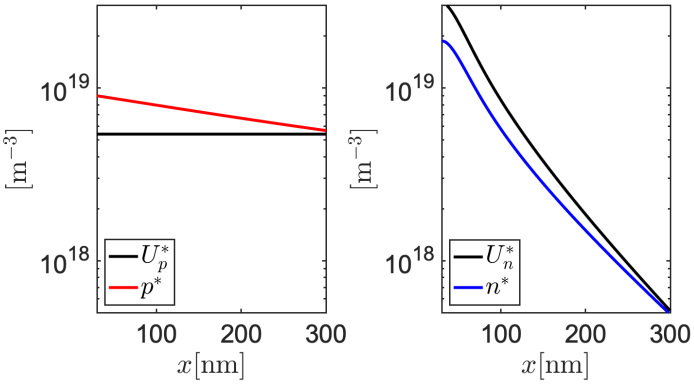

Figure 9. Left panel: hole number density in the NP region (in red color: p, in black color: u_p). Right panel: electron number density in the NP region (in blue color: n, in black color: u_n).

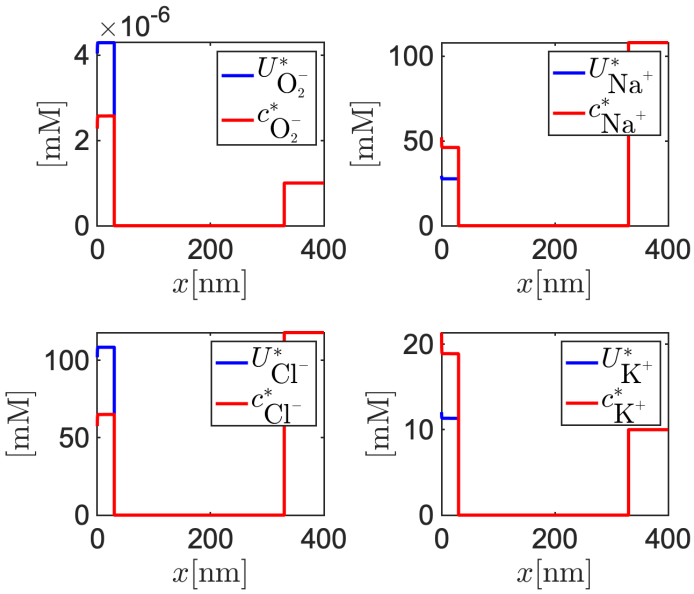

Figure 10. Piecewise electrolytic ion profiles simulated in the three regions of the computational domain Ω. In each panel, $c_\alpha = u_\alpha = 0$ in the NP region Ω_2. Top left panel: $c_{O_2^-}$ (red color) and $u_{O_2^-}$ (blue color). Top right panel: c_{Na^+} (red color) and u_{Na^+} (blue color). Bottom left panel: c_{Cl^-} (red color) and u_{Cl^-} (blue color). Bottom right panel: c_{K^+} (red color) and u_{K^+} (blue color).

7.3. The role of light intensity

In our model description of the bio-hybrid system, the presence of an electrolytic solution in the cleft screens the polarization and the Dember Effect of the NP very efficiently but does not affect the chemical role of O_2^-, which, as a Reactive Oxygen Species (ROS), may possibly trigger some signaling pathways at the neuron membrane.

Figure 11 represents the predicted superoxide molar density at the neuron membrane, for different values of light intensity impinging onto the NP. As light intensity becomes higher than 1 W m^{-2}, the dependence between the superoxide molar density at the neuron membrane and the light intensity becomes almost linear in the logarithmic scale. Below this threshold value, instead, the superoxide molar density tends to a plateu value, coinciding with the equilibrium concentration of O_2^- in the aqueous solution, which is assumed to be around 1 nM. From the data reported in [1], the light intensity regime hitting the retinal layers under sunlight exposure is of 0.2 W m^{-2}, which corresponds in Figure 11 to a value of superoxide molar density of a few nM, likely a too small molar density to trigger any photochemical effect at the neuron membrane.

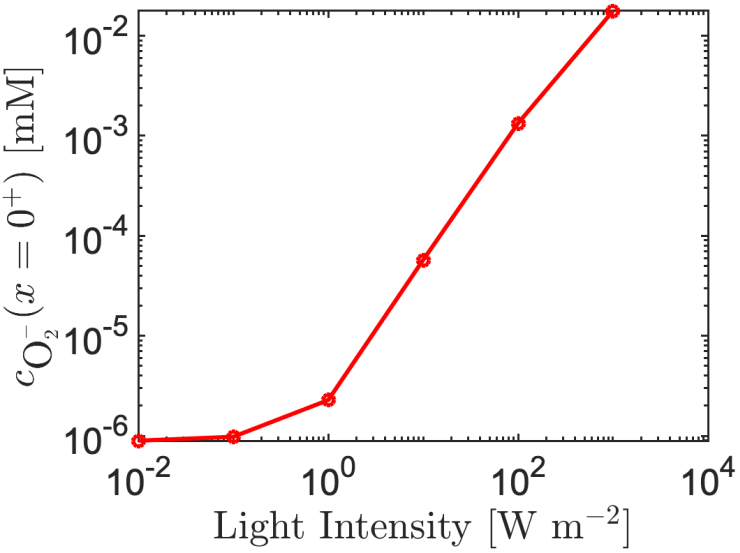

Figure 11. Superoxide molar density $c_{O_2^-}(x = 0^+)$ at the neuron membrane as a function of the light intensity impinging onto the NP.

The increase in light intensity not only affects the efficiency of the interface reactions leading to the production of O_2^-, but has also some numerical consequences. Figure 12 represents the number of Gummel's Map iterations that are required to meet a tolerance $\delta = 10^{-5}$ as a function of light intensity. When light intensity exceeds 10 W m^{-2} we observe that the convergence of the algorithm is significantly deteriorated and the number of iterations abruptly becomes three times larger than in the lower light intensity regime. This may be explained by the increased rate of nonlinear interface reactions, which, correspondingly, gives rise to an increase of the coupling between continuity equations and NLP equation, resulting into a reduced convergence rate of the Gummel Map. This behavior agrees favorably with similar conclusions drawn in [18] and [12] in the application of Gummel's Map to semiconductor device simulation.

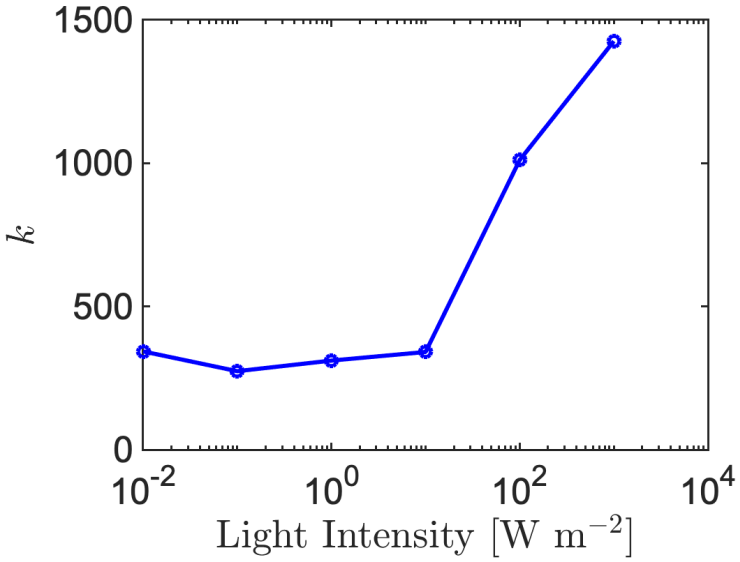

Figure 12. Number of Gummel's Map iterations as a function of the light intensity impinging onto the NP.

8. Proof of Theorem 5.1

In this section we provide the full details of the proof of Theorem 5.1.

The adopted notation is:

$$\begin{aligned} u_\alpha,\ \alpha &= Na^+, Cl^-, K^+,\ z_\alpha = +1, -1, +1, \text{ respectively;} \\ u &= u_{O_2^-},\ u_p \text{ and } u_n \text{ for the carriers;} \\ \psi &\quad \text{is the electric potential.} \end{aligned}$$

8.1. Strategy for the existence of a solution: the Gummel Map

The strategy to prove the existence of a solution of the fully coupled nonlinear differential model constituted by the boundary value problems (3.1), (3.8), (3.12) and (3.16), consists in constructing a solution map, henceforth referred to as Gummel's Map in analogy to that used in the case of the Drift-Diffusion model for semiconductor devices [10], acting over some convex, closed subsets of suitable Sobolev spaces and showing that this map has a fixed point.

As illustrated in Section 5.1, the Gummel Map is a composition of two other maps: the first map, $\mathcal{T}$, determines the potential $\psi^{(1)}$ once the other variables $u_\alpha^{(0)}, u^{(0)}, u_n^{(0)}, u_p^{(0)}$ have been fixed. The differential problem for $\psi^{(1)}$ is nonlinear (cf. (4.1a) with $k = 0$) and to solve it we shall use the Leray-Schauder Theorem. Once $\psi^{(1)}$ has been uniquely determined, still keeping the same $u_\alpha^{(0)}, u^{(0)}, u_n^{(0)}, u_p^{(0)}$, a second map, $\mathcal{P}$, computes a set of new variables $u_\alpha^{(1)}, u^{(1)}, u_n^{(1)}, u_p^{(1)}$. The problems for all these variables are all linear and the main tool will be the Lax-Milgram Theorem. The Gummel Map is precisely $\mathbb{G} = \mathcal{P} \circ \mathcal{T}$ and it turns out (Schauder Theorem) that it has a fixed point, which is a solution of the original nonlinear fully coupled problem constituted by the boundary value problems (3.1), (3.8), (3.12) and (3.16).

8.2. The map $\mathcal{T} : \left(u_\alpha^{(0)}, u^{(0)}, u_n^{(0)}, u_p^{(0)}\right) \to \psi^{(1)}$

In this section, we study the mathematical properties of the map that represents the step to update the electric potential in the Gummel Map. We assume that $u_\alpha^{(0)}$, $\alpha = Na^+, Cl^-, K^+$, and $u^{(0)}$ are given in $H^1(\Omega_{1,3})$, $u_n^{(0)}, u_p^{(0)}$ are given in $H^1(\Omega_2)$ and that they are all *nonnegative.* To solve the nonlinear Poisson equation (4.1a) for $\psi^{(1)}$ we will use a variational formulation and the Lax-Milgram Theorem. To this purpose, let us consider the space V defined in (5.5a). In V we introduce the following scalar product (see Lemma 8.1):

$$(v, w)_V = \sum_{j=1}^{3} \int_{\Omega_j} v'w' + v(0)\, w(0) + \left(v\left(R_1^+\right) - v\left(R_1^-\right)\right)\left(w\left(R_1^+\right) - w\left(R_1^-\right)\right) \tag{8.1}$$
$$+ \left(v\left(R_2^+\right) - v\left(R_2^-\right)\right)\left(w\left(R_2^+\right) - w\left(R_2^-\right)\right)$$

wih energy norm

$$\|v\|_V^2 = \sum_{j=1}^{3} \int_{\Omega_j} (v')^2 + v(0)^2 + \left(v\left(R_1^+\right) - v\left(R_1^-\right)\right)^2 + \left(v\left(R_2^+\right) - v\left(R_2^-\right)\right)^2. \tag{8.2}$$

Lemma 8.1. (8.1) *is a scalar product in V and the norm* $\|v\|_V$ *is equivalent to the norm*

$$\|v\|^2 = \sum_{j=1}^{3} \int_{\Omega_j} (v')^2 + \|v\|_{L^2(\Omega)}^2. \tag{8.3}$$

Moreover, V is a Hilbert space with respect to the scalar product (8.1)*.*

Proof. (8.1) is bilinear, symmetric and $(v, v) \geq 0$. If $(v, v) = 0$ then v is constant on every Ω_j, and $v(0) = 0$, $v\left(R_1^+\right) = v\left(R_1^-\right)$ $v\left(R_2^+\right) = v\left(R_2^-\right)$. Since $v(0) = v(1) = 0$, then $v = 0$ on $\Omega_1 \cup \Omega_3$. In particular $v\left(R_2^+\right) = 0$ so that also $v\left(R_2^-\right) = 0$ from which $v = 0$ on Ω_2 too. Thus (8.1) is a scalar product. For the equivalence of the norms (8.2) and (8.3) it is enough to prove that there exists a constant C_L such that

$$\|v\|_{L^2(\Omega)}^2 \leq C_L \|v\|_V^2 \qquad \forall v \in V. \tag{8.4}$$

By contradiction, let $\{v_k\} \subset V$ such that, for $k \geq 1$,

$$\int_\Omega v_k^2 \geq k \left[\sum_{j=1}^{3} \int_{\Omega_j} (v_k')^2 + v_k(0)^2 + \left(v_k\left(R_1^+\right) - v_k\left(R_1^-\right)\right)^2 + \left(v_k\left(R_2^+\right) - v_k\left(R_2^-\right)\right)^2\right].$$

Normalizing, we can assume that $\|v_k\|_{L^2(\Omega)} = 1, \forall k \geq 1$. Then, in particular $\{v_k\}$ is bounded in $H^1\left(\Omega_j\right)$, $j = 1, 2, 3$ and

$$\int_{\Omega_j} (v_k')^2 + v_k(0)^2 + \left(v_k\left(R_1^+\right) - v_k\left(R_1^-\right)\right)^2 + \left(v_k\left(R_2^+\right) - v_k\left(R_2^-\right)\right)^2 \leq \frac{1}{k}. \tag{8.5}$$

From Rellich theorem, there exists a sequence $\{v_{k_m}\}$such that

$$v_{k_m} \rightharpoonup v \quad \text{in } H^1\left(\Omega_j\right),\ j = 1, 2, 3$$

$$v_{k_m} \rightarrow v \quad \text{in } L^2(\Omega).$$

The weak lower semicontinuity of the norm gives

$$\left(\int_{\Omega_j} (v')^2\right)^{1/2} \leq \liminf \left(\int_{\Omega_j} (v'_{k_m})^2\right)^{1/2} = 0$$

and hence v is constant in $\Omega_1, \Omega_2, \Omega_3$. In particular, $v = 0$ in Ω_3, since $v(1) = 0$, and therefore $v_{k_m}\left(R_2^+\right) \rightarrow 0$. From (8.5) we deduce that $v_{k_m}\left(R_2^+\right) - v_{k_m}\left(R_2^-\right) \rightarrow 0$ so that also $v_{k_m}\left(R_2^-\right) \rightarrow 0$ which implies $v = 0$ in Ω_2. Finally, again from (8.5), $v_{k_m}(0) \rightarrow v(0) = 0$ and hence $v = 0$ in Ω_1. Thus $v = 0$ in Ω, while $\|v_k\|_{L^2(\Omega)} = 1 \rightarrow \|v\|_{L^2(\Omega)}$: contradiction. □

Corollary 8.2. *Let*

$$C^* = \left\{v : \overline{\Omega} \rightarrow \mathbb{R}; v_{|\Omega_j} \in C\left(\overline{\Omega}_j\right),\ j = 1,2,3\right\}$$

with the norm

$$\|v\|_{C^*} = \sum_{j=1}^{3} \max_{\overline{\Omega}_j} |v|.$$

Then

$$\|v\|_{C^*} \leq C_I \|v\|_V \qquad \forall v \in V \tag{8.6}$$

with compact embedding $V \hookrightarrow C^*$.

In view of the weak formulation of the NLP equation, we introduce the bilinear form

$$\begin{aligned} B(\psi,\varphi) \;=\; & \sum_{j=1}^{3} \varepsilon_j \int_{\Omega_j} \psi'\varphi' + C_m^0 \psi(0)\varphi(0) + C_m\left(\psi\left(R_1^-\right) - \psi\left(R_1^+\right)\right)\varphi\left(R_1^-\right) \\ & + C_m\left(\psi\left(R_2^-\right) - \psi\left(R_2^+\right)\right)\varphi\left(R_2^-\right) + C_m(\psi\left(R_1^+\right) - \psi\left(R_1^-\right))\varphi\left(R_1^+\right) \\ & + C_m\left(\psi\left(R_2^{+-}\right) - \psi\left(R_2^-\right)\right)\varphi\left(R_2^+\right). \end{aligned}$$

It is easy to check that $B : V \times V \rightarrow \mathbb{R}$ is continuous. Moreover

$$B(\psi,\psi) \;=\; \sum_{j=1}^{3} \varepsilon_j \int_{\Omega_j} (\psi')^2 + C_m^0 \psi(0)^2 + C_m\left(\psi\left(R_1^-\right) - \psi\left(R_1^+\right)\right)^2 + C_m\left(\psi\left(R_2^-\right) - \psi\left(R_2^+\right)\right)^2$$

whence

$$B(\psi,\psi) \geq \min\left\{\varepsilon_j, C_m^0, C_m\right\} \|\psi\|_V^2$$

which shows the coercivity of B on V.

For fixed, nonnegative, $u_\alpha^{(0)}, u^{(0)}, u_n^{(0)}, u_p^{(0)}$, let us consider the nonlinear problem of finding $\psi \in V$ such that

$$B(\psi,\varphi) = \int_\Omega \lambda^{-2} f^0(x,\psi)\varphi + C_m^0 \psi_N \varphi(0) \qquad \forall \varphi \in V. \tag{8.7}$$

where

$$f^0(x,0) = \begin{cases} \gamma_1\left(\sum_\alpha z_\alpha u_\alpha^{(0)} - u^{(0)} + \rho_1\right) & \text{in } \Omega_1 \\ \gamma_2\left(u_p^{(0)} - u_n^{(0)} + \rho_2\right) & \text{in } \Omega_2 \\ \gamma_1\left(\sum_\alpha z_\alpha u_\alpha^{(0)} - u^{(0)} + \rho_3\right) & \text{in } \Omega_3. \end{cases}$$

Theorem 8.3. *There exists a unique solution* $\psi^{(1)} = \mathcal{T}\left(u_\alpha^{(0)}, u^{(0)}, u_n^{(0)}, u_p^{(0)}\right) \in V$ *to (8.7) satisfying*

$$\max_{x\in\Omega} |\psi^{(1)}(x)| \le \left\|\psi^{(1)}\right\|_{C^*} \le C_I \left\|\psi^{(1)}\right\|_V \le M, \tag{8.8a}$$

where

$$M = \frac{\max\{1, C_L\} C_I}{\min\left\{\varepsilon_j, C_m^0, C_m\right\}} (C_m^0 |\psi_N| + \lambda^{-2} \left\|f^0(x,0)\right\|_{L^2(\Omega)}). \tag{8.8b}$$

We also have $\psi^{(1)} \in H^2\left(\Omega_j\right)$, $j = 1,2,3$, *and therefore* $(\psi^{(1)})' \in C^*$. *In particular,* $\mathcal{T}$ *is compact in both the topologies of* V *and* C^*. *An alternate estimate for* $\psi^{(1)}$, *possibly more convenient than* (8.8a), *is*

$$\max_{x\in\Omega} |\psi^{(1)}(x)| \le \left\|\psi^{(1)}\right\|_{C^*} \le M_1, \tag{8.8c}$$

where:

$$M_1 = \frac{C_I \max\{1, C_L\}}{\min\left\{\varepsilon_j, C_m^0, C_m\right\}} (K_1 + K_2 + K_3), \tag{8.8d}$$

$$K_1 = C_m^0 |\psi_N| + \lambda^{-2}\gamma_1 \|\rho\|_{L^\infty(\Omega_{1,3})} + \lambda^{-2}\gamma_2 \|\rho_2\|_{L^\infty(\Omega_2)} + 2\lambda^{-2}\gamma_1 \left\| \sum_{\alpha\neq O_2^-} z_\alpha u_\alpha^{(0)} \right\|_{L^\infty(\Omega_{1,3})} \tag{8.8e}$$

$$K_2 = \lambda^{-2}\gamma_2 (R_2 - R_1) \left\|u_n^{(0)} - u_p^{(0)}\right\|_{L^\infty(\Omega_2)} \tag{8.8f}$$

$$K_3 = \lambda^{-2}\gamma_1 \left\|u^{(0)}\right\|_{L^1(\Omega_{1,3})}. \tag{8.8g}$$

Proof. (Existence and regularity of a solution) We use the Leray-Schauder fixed point Theorem. Fix $\psi^* \in C^*$; the linear problem

$$B(\psi, \varphi) = \int_\Omega \lambda^{-2} f^0(x, \psi^*)\varphi + C_m^0 \psi_N \varphi(0) \qquad \forall \varphi \in V$$

has a unique solution $\psi = S(\psi^*) \in V \hookrightarrow C^*$, by Lax Milgram Theorem. The operator $S : C^* \to C^*$ is *continuous*, as it is easy to check, and *compact* (from Corollary 8.2).

To conclude, we need an apriori estimate for the solutions of the family of equations

$$\psi = sS(\psi) \qquad s \in (0,1],$$

that is of

$$B(\psi, \varphi) = s \int_\Omega \lambda^{-2} f^0(x, \psi)\varphi + C_m^0 \psi_N \varphi(0) \qquad \forall \varphi \in V,$$

of the type

$$\|\psi\|_{C^*} \le M,$$

with M independent of s and ψ.

First observe that, since the functions $u_\alpha^{(0)}, u^{(0)}, u_n^{(0)}, u_p^{(0)}$ are nonnegative, the map $\psi \longmapsto f^0(x,\psi) - f^0(x,0)$ is decreasing and hence

$$(f^0(x,\psi) - f^0(x,0))\psi \le 0 \qquad \forall \psi \in V, x \in \Omega.$$

Choosing $\varphi = \psi$, we find

$$B(\psi,\psi) - \underbrace{s\lambda^{-2}\int_\Omega (f^0(x,\psi) - f^0(x,0)\,\psi}_{\leq 0} = s\int_\Omega (\lambda^{-2} f^0(x,0)\,\psi + C_m^0 \psi_N \psi\,(0)$$

from which

$$\min\left\{\varepsilon_j, C_m^0, C_m\right\}\|v\|_V^2 \leq \left(C_m^0\,|\psi_N| + \lambda^{-2}\left\|f^0(x,0)\right\|_{L^2(\Omega)}\right)\max\{1, C_L\}\,\|\psi\|_{V(\Omega)}$$

and

$$\|v\|_{C^*} \leq \frac{C_I \max\{1, C_L\}}{\min\left\{\varepsilon_j, C_m^0, C_m\right\}}\left(C_m^0\,|\psi_N| + \lambda^{-2}\left\|f^0(x,0)\right\|_{L^2(\Omega)}\right).$$

The H^2-regularity follows directly from the differential equation. □

Proof. (Uniqueness of the solution) Let η, ψ be solutions to (8.7). Then $w = \psi - \eta$ solves the equation

$$B(w,\varphi) = \lambda^{-2}\int_\Omega (f^0(x,\psi) - f^0(x,\eta))\varphi \qquad \forall \varphi \in V.$$

Letting $\varphi = w$ we get,

$$B(w,w) = \lambda^{-2}\int_\Omega (f^0(x,\psi) - f^0(x,\eta))(\psi - \eta) \leq 0$$

from which $w = 0$. By the Leray-Schauder Theorem, the map S has a unique fixed point ψ^0. This fixed point is the unique weak solution to problem (8.7) and satisfies the estimate (8.8a). This concludes the proof of Theorem 8.3. □

8.3. The map $\mathcal{P} : (\psi^1, u_\alpha^{(0)}, u^{(0)}, u_n^{(0)}, u_p^{(0)}) \to (u_\alpha^{(1)}, u^{(1)}, u_n^{(1)}, u_p^{(1)})$

In this section, we study the mathematical properties of the map that represents the step to update the ion molar densities and the carrier number densities in the Gummel Map.

8.3.1. Determining u_α^1, $\alpha = Na^+, Cl^-, K^+$

Given $\psi^{(1)}$ as uniquely determined in Theorem 8.3, in this subsection we solve problem (3.8a)–(3.11g). For notational simplicity, we denote $u_\alpha^{(1)}$ by u_α and $\psi^{(1)}$ by ψ.

Consider first the problem in Ω_1. In $H^1(\Omega_1)$ we use the norm (equivalent to the usual one)

$$\|u_\alpha\|_{H_\alpha^1(\Omega_1)}^2 = \int_{\Omega_1} (u_\alpha')^2 + u_\alpha^2(0).$$

The weak formulation of our problem is the following. *To find $u_\alpha \in H^1(\Omega_1)$ such that, for every $v \in H^1(\Omega_1)$*

$$A_1(u_\alpha, v) = \int_{\Omega_1} D_\alpha^1 e^{-z_\alpha \psi(R_2^+)} u_\alpha' v' \tag{8.9}$$

$$+ P_{\alpha,i}Be\left(-\Psi_{\alpha,i}\right)e^{-z_\alpha\psi\left(R_1^-\right)}u_\alpha\left(R_1^-\right)v\left(R_1^-\right) + P_\alpha Be\left(\Psi_\alpha\right)e^{-z_\alpha\psi(0)}u_\alpha\left(0\right)v\left(0\right)$$
$$= P_{\alpha,i}Be\left(\Psi_{\alpha,i}\right)e^{-z_\alpha\psi\left(R_2^+\right)}u_\alpha^{(0)}\left(R_2^+\right)v\left(R_1^-\right) + P_\alpha Be\left(-\Psi_\alpha\right)e^{-z_\alpha\psi_N}u_{\alpha,N}v(0).$$

It is immediate to see that the bilinear form $A_1 : H^1\left(\Omega_1\right) \times H^1\left(\Omega_1\right)$ is continuous. Moreover

$$A_1\left(u_\alpha, u_\alpha\right) = \int_{\Omega_1} D_\alpha^1 e^{-z_\alpha\psi\left(R_2^+\right)}\left(u_\alpha'\right)^2 + P_{\alpha,i}Be\left(-\Psi_{\alpha,i}\right)e^{-z_\alpha\psi\left(R_1^-\right)}u_\alpha^2\left(R_1^-\right) + P_\alpha Be\left(\Psi_\alpha\right)e^{-z_\alpha\psi(0)}u_\alpha^2\left(0\right)$$
$$= P_{\alpha,i}Be\left(\Psi_{\alpha,i}\right)e^{-z_\alpha\psi^0\left(R_2^+\right)}u_\alpha^{(0)}\left(R_2^+\right)u_\alpha\left(R_1^-\right) + P_\alpha Be\left(-\Psi_\alpha\right)e^{-z_\alpha\psi_N}u_{\alpha,N}u_\alpha(0).$$

Since $Be\left(2M\right) \leq Be\left(\pm\Psi_\alpha\right) \leq Be\left(-2M\right)$ we find

$$A_1\left(u_\alpha, u_\alpha\right) \geq e^{-M}\min\left\{D_\alpha^1, P_\alpha Be\left(2M\right)\right\}\left\{\int_{\Omega_1}\left(u_\alpha'\right)^2 + u_\alpha^2\left(0\right)\right\}$$
$$= e^{-M}\min\left\{D_\alpha^1, P_\alpha Be\left(2M\right)\right\}\left\|u_\alpha\right\|^2_{H^1_\alpha(\Omega_1)},$$

and therefore A_1 is coercive in $H^1\left(\Omega_1\right)$. Since

$$v \mapsto P_{\alpha,i}Be\left(\Psi_{\alpha,i}\right)e^{-z_\alpha\psi\left(R_2^+\right)}u_\alpha^{(0)}\left(R_2^+\right)v\left(R_1^-\right) + P_\alpha Be\left(-\Psi_\alpha\right)e^{-z_\alpha\psi_N}u_{\alpha,N}v(0)$$

is an element of $H^1\left(\Omega_1\right)^*$ (the dual of $H^1\left(\Omega_1\right)$), the following result holds.

Theorem 8.4. *There exists a unique solution $u_\alpha^1 \in H^1\left(\Omega_1\right)$ of problem (8.9) and*

$$\left\|u_\alpha^1\right\|_{H^1_\alpha(\Omega_1)} \leq \frac{e^{2M}Be\left(-2M\right)}{\min\left\{D_\alpha^1, P_\alpha Be\left(2M\right)\right\}}\left\{P_{\alpha,i}u_\alpha^{(0)}\left(R_2^+\right) + P_\alpha u_{\alpha,N}\right\}. \tag{8.10}$$

Moreover $u_\alpha^1 \in H^3\left(\Omega_1\right)$, u_α^1 takes its maximum and minimum at $x = 0$ or $x = R_1$ and

$$0 < u_\alpha^1 \leq \max\left\{u_{\alpha,N}, u_\alpha^{(0)}\left(R_2^+\right)\right\}. \tag{8.11}$$

Proof. For notational simplicity, we denote u_α^1 by u_α. Existence, uniqueness and the stability estimate (8.10) follow from Lax-Milgram Theorem. The regularity follows directly from the differential equation that can be written in the form

$$-u_\alpha''\left(x\right) + \psi'\left(x\right)u_\alpha'\left(x\right) = 0.$$

Since ψ' is bounded and continuous, u_α attains maximum and minimum at the endpoints of Ω_1, by the maximum principle.

If $u_\alpha\left(0\right) = \min u_\alpha \leq 0$, then, by the Hopf principle, $u_\alpha'\left(0\right) > 0$, while if $u_\alpha\left(R_1^-\right) = \min u_\alpha \leq 0$, then $u'\left(R_1^-\right) < 0$. In both cases we get a contradiction with the Robin conditions. Thus $u_\alpha > 0$.

Let $\max u_\alpha = u_\alpha\left(0\right)$. Then the Hopf principle gives $u_\alpha'\left(0\right) < 0$ and from the Robin condition we find

$$u_\alpha\left(0\right) \leq \frac{Be\left(-\Psi_\alpha\right)}{Be\left(\Psi_\alpha\right)}e^{-\Psi_\alpha}u_{\alpha,N} = u_{\alpha,N}$$

since

$$\frac{Be\left(-\Psi_\alpha\right)}{Be\left(\Psi_\alpha\right)}e^{-\Psi_\alpha}=1.$$

On the other hand, if $\max u_\alpha = u_\alpha\left(R_1^-\right)$, from the Hopf principle we deduce $u'_\alpha\left(R_1^-\right)>0$ and from the Robin condition we get

$$u_\alpha\left(R_1^-\right)\leq\frac{Be\left(\Psi_{\alpha,i}\right)}{Be\left(-\Psi_\alpha\right)}e^{\Psi_\alpha}u_{\alpha,N}=u_\alpha^{(0)}\left(R_2^+\right)$$

since

$$\frac{Be\left(\Psi_{\alpha,i}\right)}{Be\left(-\Psi_\alpha\right)}=1.$$

□

Consider now the problem in Ω_3 for v_α. Its weak formulation reads:
To find $v_\alpha\in H^1_{0,\{1\}}\left(\Omega_3\right)$ *such that, for every* $\eta\in H^1_{0,\{1\}}\left(\Omega_3\right)$,

$$\begin{aligned}A_3\left(v_\alpha,\eta\right) &= \int_{\Omega_1}D_\alpha^3e^{-z_\alpha\psi\left(R_2^+\right)}v'_\alpha\eta'+P_{\alpha,i}Be\left(\Psi_{\alpha,i}\right)e^{-z_\alpha\psi\left(R_2^+\right)}v_\alpha(R_2^+)\eta(R_2^+) \\ &= P_{\alpha,i}Be\left(-\Psi_{\alpha,i}\right)e^{-z_\alpha\psi\left(R_1^-\right)}u_\alpha^{(0)}\left(R_1^-\right)\eta\left(R_2^+\right)-P_{\alpha,i}Be\left(\Psi_{\alpha,i}\right)e^{-z_\alpha\psi\left(R_2^+\right)}\overline{u}_\alpha\eta\left(R_2^+\right).\end{aligned}\tag{8.12}$$

It is immediate to see that the bilinear form $A_3:H^1_{0,\{1\}}\left(\Omega_3\right)\times H^1_{0,\{1\}}\left(\Omega_3\right)\to\mathbb{R}$ is continuous. Moreover

$$A_3\left(v_\alpha,v_\alpha\right)\geq e^{-M}D_\alpha^3\int_{\Omega_3}\left(v'_\alpha\right)^2=e^{-M}D_\alpha^3\left\|v_\alpha\right\|^2_{H^1_{0,\{1\}}\left(\Omega_3\right)}$$

and A_3 is also coercive. The following result holds.

Theorem 8.5. *There exists a unique solution* $v_\alpha\in H^1_{0,\{1\}}\left(\Omega_3\right)$ *of problem (8.12) and*

$$\left\|v_\alpha\right\|_{1,0}\leq\frac{e^{2M}Be\left(-2M\right)P_{\alpha,i}}{D_\alpha^3}\overline{u}_\alpha.\tag{8.13}$$

As a consequence, there exists a unique solution $u_\alpha^1=v_\alpha+\overline{u}_\alpha$ *of the original problem. Moreover,* $u_\alpha^1\in H^3\left(\Omega_3\right)$, u_α^1 *attains its maximum and minimum at* $x=0$ *or* $x=R_2$ *and*

$$0<u_\alpha^1\leq\max\left\{\overline{u}_\alpha,u_\alpha^{(0)}\left(R_1^-\right)\right\}.\tag{8.14}$$

Proof. The proof follows the same lines as the proof of Theorem 8.4. □

Remark 8.1. *From the definition* (5.6a)*,* X_α is a closed, convex and bounded subset of C^* and if $u_\alpha^{(0)}\in X_\alpha$ then

$$u\in\left\{u_\alpha:0<u_\alpha\leq\max\left\{u_{\alpha,N},\bar{u}_\alpha\right\}\right\}.$$

8.3.2. Determining $u^1 = u^{(1)}_{O_2^-}$

In this section we solve problem (3.12a)–(3.15d) where we denote $\psi^{(1)}$ by ψ. With this aim, we introduce the bilinear form $E : H^1(\Omega_{1,3}) \times H^1(\Omega_{1,3}) \to \mathbb{R}$ defined as

$$E(u,v) = \int_{\Omega_{1,3}} D(x)\, e^{\psi^0} u'v' + \int_{\Omega_{1,3}} \frac{k_1 \tilde{C}\, e^{-\psi^0}}{C^{EQ}} uv + k_p e^{\left[\psi(R_1^-)-\psi(R_1^+)\right]} u_p^{(0)}(R_1^+)\, u(R_1^-)\, v(R_1^-)$$
$$+ k_p e^{\left[\psi(R_2^+)-\psi(R_2^-)\right]} u_p^{(0)}(R_2^-)\, u(R_2^+)\, v(R_2^+),$$

where $D = D(x)$ is defined in (3.12b).

We want *to find* $u^1 \in H^1(\Omega_{1,3})$ *such that, for all* $v \in H^1(\Omega_{1,3})$,

$$E\left(u^1, v\right) = k_1 \tilde{C} \int_{\Omega_{1,3}} v + k_n u_n^{(0)}(R_1^+)\, e^{\psi\left(R_1^+\right)} e^{-g\left(\psi(R_1^-), u^{(0)}(R_1^-)\right)} v(R_1^-) \tag{8.15}$$
$$+ k_n e^{\psi\left(R_2^-\right)} u_n^{(0)}(R_2^-)\, e^{-g\left(\psi(R_2^+), u^{(0)}(R_2^+)\right)} v(R_2^+).$$

The bilinear form E is symmetric, continuous and coercive in $H^1(\Omega_{1,3})$ with coercivity constant δe^{-M} where

$$\delta = \min\left\{D, \frac{k_1 \tilde{C}}{C^{EQ}}\right\}. \tag{8.16}$$

The following result holds.

Theorem 8.6. *There exists a unique solution* $u^1 \in H^1(\Omega_{1,3})$ *of problem (8.15) and the following stability estimates hold:*

$$\left\|u^1\right\|_{H^1(\Omega_{1,3})} \leq M_u, \tag{8.17}$$
$$\left\|u^1\right\|_{L^1(\Omega_{1,3})} \leq \mathcal{K}_u, \tag{8.18}$$

where:

$$M_u = \frac{C_I e^M}{\delta}\left\{k_n e^M \max\left\{u_n^{(0)}(R_1^+), u_n^{(0)}(R_2^-)\right\} + k_1 \tilde{C}\right\}, \tag{8.19}$$

$$\mathcal{K}_u = C^{EQ} e^M \left\{\frac{k_n e^M \max\left\{u_n^{(0)}\left(R_1^+\right), u_n^{(0)}\left(R_2^-\right)\right\}}{k_1 \tilde{C}} + 1\right\}. \tag{8.20}$$

Moreover, $u^1 > 0$ *in* $\Omega_{1,3}$ *and* $u^1 \in H^3(\Omega_{1,3})$.

Proof. The existence and uniqueness of the solution, as well as the stability estimates (8.17), (8.18), follow from Lax Milgram Theorem. The H^3-regularity follows directly from the differential equation. For notational simplicity set $u \equiv u^1$. To show that $u > 0$, write the differential equation in the form.

$$-D_j e^{\psi(x)} u''(x) - D_j e^{\psi(x)} \psi'(x)\, u'(x) + \frac{k_1 \tilde{C}\, e^{-\psi}}{C^{EQ}} u = k_1 \tilde{C} > 0 \quad \text{in } \Omega_j,\ j = 1, 3.$$

If $x_0 \in \Omega_{1,3}$ is a point of minimum, then $u''(x_0) \geq 0, u'(x_0) = 0$. Thus it cannot be $u(x_0) \leq 0$. Also it cannot be $\min u = u(0) \leq 0$, since then, by Hopf principle, $u'(0) > 0$, while we have $u'(0) = 0$. If

$\min u = u\left(R_1^-\right) \leq 0$, Hopf principle gives $u'\left(R_1^-\right) < 0$ in contradiction with the Robin condition. Thus $\min_{\overline{\Omega}_1} u > 0$. Similarly, it cannot be $\min u = u(1) \leq 0$ since $u'(1) = 0$; finally, if $\min u = u\left(R_2^-\right) \leq 0$, Hopf principle gives $u'\left(R_2^-\right) > 0$ in contradiction with the Robin condition. Thus, also $\min_{\overline{\Omega_3}} u > 0$. □

Remark 8.2. *We assume that* $u_n^{(0)} \leq N = G_{max}\tau_{max} \sim 10^9$*, and that*

$$\beta = \frac{C^{EQ}k_n}{k_1\tilde{C}}e^{M_1+M_2}$$

is sufficiently small. Then, we have

$$\left\|u^1\right\|_{H^1(\Omega_{1,3})} \leq \mathcal{M}_u, \tag{8.21}$$

where

$$\mathcal{M}_u = \frac{C_I e^M}{\delta}\left\{N\,k_n e^M + k_1\tilde{C}\right\}, \tag{8.22}$$

and, for a suitable K_3 *depending only on* β, N *and* λ*, (see the definition (8.8g))*

$$\lambda^{-2}\gamma_1\left\|u^1\right\|_{L^1(\Omega_{1,3})} \leq K_3. \tag{8.23}$$

To complete the analysis for the superoxide molar density, we need a bound from below for u. In this direction, the following result holds.

Lemma 8.7. *Let* $u^1(x_{\min}) = \min_{\overline{\Omega}_1\cup\overline{\Omega}_3} u^1$*. If a)* $x_{\min} \in \Omega_1 \cup \Omega_3$ *or b)* $x_{\min} = 0$ or $x_{\min} = 1$*, then*

$$u^1(x_{\min}) \geq C^{EQ}e^{-M}. \tag{8.24}$$

Proof. **a)** If $x_{\min} \in \Omega_1 \cup \Omega_3$, directly from the differential equation we get $u^1(x_{\min}) \geq C^{EQ}e^{\psi(x_{\min})} \geq C^{EQ}e^{-M}$. **b)** If $x_{\min} = 0$, since $(u^1)'(0) = 0$, upon integrating the differential equation over $(0, \varepsilon_k)$ yields

$$D_1 e^{\psi(x)}(u^1)'(\varepsilon_k) = \int_0^{\varepsilon_k}\frac{k_1\tilde{C}}{C^{EQ}}(u^1e^{-\psi} - C^{EQ}) \geq 0,$$

at least along a sequence $\varepsilon_k \to 0$, otherwise there should exist an interval $(0, \varepsilon)$ where $(u^1)' < 0$. Thus we deduce that $u^1(0)\,e^{-\psi(0)} - C^{EQ} < 0$ and therefore $u^1(0) \geq C^{EQ}e^{\psi(0)} \geq C^{EQ}e^{-M}$. If $x_{\min} = 1$, after integration over $(\varepsilon_k, 1)$ we have

$$-D_1 e^{\psi(\varepsilon_k)}(u^1)'(\varepsilon_k) = \int_{\varepsilon_k}^1\frac{k_1\tilde{C}}{C^{EQ}}(u^1e^{-\psi} - C^{EQ}) \geq 0,$$

at least along a sequence $\varepsilon_k \to 1$. Therefore it cannot be $u^1(1)\,e^{-\psi(1)} - C^{EQ} < 0$ so that $u^1(1) \geq C^{EQ}e^{\psi(1)} \geq C^{EQ}e^{-M}$. This completes the proof. □

8.3.3. Determining the carriers u_p^1, u_n^1

In this section we solve problems (3.16a)–(3.19d) where we denote $\psi^{(1)}$ by ψ. We additionally assume that $N \geq u_n^{(0)} \geq m_n > 0$ and $N \geq u_p^{(0)} \geq m_p > 0$, where m_n, m_p are not specified yet. The weak formulation for problems (3.16a)–(3.19d) reads:
To find $u_n, u_p \in H^1(\Omega_2)$ such that for all $\forall \varphi \in H^1(\Omega_2)$

$$\int_{\Omega_2} D_n e^{\psi} u_n' \varphi' + \int_{\Omega_2} \frac{u_p^{(0)} u_n \varphi}{\tau_p(u_n e^{\psi} + 1) + \tau_n(u_p^{(0)} e^{-\psi} + 1)} + \frac{n_r}{n_i} k_n e^{\psi(R_2^-)} e^{-g\left(\psi(R_2^+), u^{(0)}(R_2^+)\right)} u_n(R_2^-) \varphi(R_2^-)$$

$$+ \frac{n_r}{n_i} k_n e^{\psi(R_1^+)} e^{-g\left(\psi(R_1^-), u^{(0)}(R_1^-)\right)} u_n(R_1^+) \varphi(R_1^+) = \int_{\Omega_2} \eta G \varphi + \int_{\Omega_2} \frac{\varphi}{\tau_p(u_n^{(0)} e^{\psi} + 1) + \tau_n(u_p^{(0)} e^{-\psi} + 1)}, \tag{8.25}$$

and

$$\int_{\Omega_2} D_p e^{-\psi} u_p' \varphi' + \int_{\Omega_2} \frac{u_n^{(0)} u_p \varphi}{\tau_p(u_n^{(0)} e^{\psi} + 1) + \tau_n(u_p^{(0)} e^{-\psi} + 1)} + \frac{n_r}{n_i} k_p u^{(0)}(R_2^+) e^{\psi(R_2^+) - \psi(R_2^-)} u_p(R_2^-) \varphi(R_2^-)$$

$$+ \frac{n_r}{n_i} k_p u^{(0)}(R_1^-) e^{\psi(R_1^-) - \psi(R_1^+)} u_p(R_1^+) \varphi(R_1^+) = \int_{\Omega_2} \eta G \varphi + \int_{\Omega_2} \frac{\varphi}{\tau_p(u_n^{(0)} e^{\psi} + 1) + \tau_n(u_p^{(0)} e^{-\psi} + 1)}. \tag{8.26}$$

Since

$$\frac{m_p}{(\tau_p + \tau_n)(N e^M + 1)} \leq \frac{u_n^{(0)}}{\tau_p(u_n^{(0)} e^{\psi} + 1) + \tau_n(u_p^{(0)} e^{-\psi} + 1)} \leq \frac{e^M}{\tau_p}$$

and

$$\frac{m_n}{(\tau_p + \tau_n)(N e^M + 1)} \leq \frac{u_n^{(0)}}{\tau_p(u_n^{(0)} e^{\psi} + 1) + \tau_n(u_p^{(0)} e^{-\psi} + 1)} \leq \frac{e^M}{\tau_p},$$

both bilinear forms in (8.25), (8.26) are continuous and coercive. The following result holds.

Theorem 8.8. *The variational problems (8.25), (8.26) have a unique solution u_n^1, u_p^1, satisfying the stability estimate*

$$\left\| u_{n,p}^1 \right\|_{H_1(\Omega_2)} \leq \frac{\sqrt{R_2 - R_1}\left(N e^M + 1\right)\left(\eta G(\tau_p + \tau_n) + 1\right)}{m_{p,n}} \equiv U_{n,p} \tag{8.27}$$

Moreover, both u_n, u_p belong to $H^3(\Omega_2)$ and:

a) u_n^1, u_p^1 are positive in Ω_2;

b) u_n^1, u_p^1 attain their maximum at a point in Ω_2 with:

$$\max u_n^1 \geq \frac{(R_2 - R_1)\eta G}{e^M(\tau_n^{-1}(R_2 - R_1) + 2\frac{n_r}{n_i} k_n)} \equiv M_n > 0 \tag{8.28}$$

$$\max u_p \geq \frac{(R_2 - R_1)\eta G}{e^M(\tau_p^{-1}(R_2 - R_1) + 2N\frac{n_r}{n_i} k_p e^M} \equiv M_p > 0. \tag{8.29}$$

Proof. a) Let $\min u_n^1 = u_n^1(x_0) \le 0$. If $x_0 \in \Omega_2$ we find the contradiction

$$0 \ge -D_n e^{\psi(x_0)}(u_n^1)''(x_0) + \frac{u_p^{(0)}(x_0)\, u_n(x_0)}{\tau_p(u_n(x_0)\, e^{\psi(x_0)} + 1) + \tau_n(u_p^{(0)}(x_0)\, e^{-\psi(x_0)} + 1)} \ge \eta G > 0.$$

If $x_0 = R_1$, from the Hopf principle we get $(u_n^1)'\left(R_1^+\right) > 0$, while if $x_0 = R_2$ we have $(u_n^1)'\left(R_2^-\right) < 0$; in both cases we get a contradiction with the Robin conditions. Thus $\min u_n^1 > 0$. The argument for u_p^1 is similar.

b) u_n^1 and u_p^1 cannot attain their (positive) maximum at an end point $x = R_1$ or $x = R_2$, because in the former case $(u_{n,p}^1)'\left(R_1^+\right) \le 0$, while in the latter case $u_{n,p}'\left(R_2^-\right) \ge 0$; both are in contrast with the Robin conditions.

The inequalities (8.28) and (8.29) follow by taking $\varphi = 1$ in (8.25) and (8.26). □

Remark 8.3. *Inserting $\varphi = u_{n,p}^1$ in the weak formulations for u_n^1 and u_p^1, we also find the estimates*

$$\int_{\Omega_2} \left(\frac{du_n^1}{dx}\right)^2 \le D_n e^M (R_2 - R_1)(\eta G + 1) \max u_n^1 \tag{8.30}$$

and

$$\int_{\Omega_2} \left(\frac{du_p^1}{dx}\right)^2 \le D_p e^M (R_2 - R_1)(\eta G + 1) \max u_p^1. \tag{8.31}$$

The following result gives a characterization of m_n and m_p.

Corollary 8.9. *If*

$$R_2 - R_1 \le \frac{1}{4} \frac{\eta G}{D_n(\eta G + 1)\, e^M \left[\tau_n^{-1} e^M((R_2 - R_1) + \frac{n_r}{n_i} k_n)\right]}, \tag{8.32}$$

then

$$u_n(x_{\min}) \ge \frac{1}{2} \frac{(R_2 - R_1)\eta G}{\tau_n^{-1} e^M((R_2 - R_1) + 2\frac{n_r}{n_i} k_n)} \equiv m_n. \tag{8.33}$$

If

$$R_2 - R_1 \le \frac{1}{4} \frac{\eta G}{D_p(\eta G + 1)\, e^M(\tau_p^{-1}(R_2 - R_1) + 2N\frac{n_r}{n_i} k_p e^M)}, \tag{8.34}$$

then

$$u_p(x_{\min}) \ge \frac{1}{2} \frac{(R_2 - R_1)\eta G}{e^M(\tau_p^{-1}(R_2 - R_1) + 2N\frac{n_r}{n_i} k_p e^M} = m_p \tag{8.35}$$

Proof. We have

$$\begin{aligned} u_n^1(x_{\max}) &= u_n^1(x_{\min}) + \int_{x_{\min}}^{x_{\max}} \frac{du_n^1}{dx} \le u_n^1(x_{\min}) + \sqrt{(R_2 - R_1)} \left(\int_{x_{\min}}^{x_{\max}} \left(\frac{du_n^1}{dx}\right)^2\right)^{1/2} \\ \text{(using (8.30))} &\le \underbrace{\sqrt{D_n(\eta G + 1)} e^{M/2}(R_2 - R_1)}_{b} \sqrt{u_n^1(x_{\max})} + u_n^1(x_{\min}) \end{aligned}$$

from which

$$u_n^1(x_{\max}) - b\sqrt{u_n^1(x_{\max})} \le u_n^1(x_{\min}). \tag{8.36}$$

Assume that, for a small ε,

$$R_2 - R_1 \leq \frac{(1-\varepsilon)^2 \eta G}{D_n (\eta G + 1) e^M \left[\tau_n^{-1} e^M ((R_2 - R_1) + 2\frac{n_r}{n_i} k_n)\right]}.$$

Then

$$u_n^1 (x_{\max}) \geq \frac{(R_2 - R_1)\eta G}{\tau_n^{-1} e^M ((R_2 - R_1) + 2\frac{n_r}{n_i} k_n)} \geq \frac{D_n (\eta G + 1) e^M (R_2 - R_1)^2}{(1-\varepsilon)^2} = \frac{b^2}{(1-\varepsilon)^2}$$

or

$$(1-\varepsilon)\sqrt{u_n^1 (x_{\max})} \geq b, \quad (1-\varepsilon) u_n^1 (x_{\max}) \geq b\sqrt{u_n^1 (x_{\max})}$$

and finally,

$$u_n^1 (x_{\max}) - b\sqrt{u_n^1 (x_{\max})} = \varepsilon u_n^1 (x_{\max}) + (1-\varepsilon) u_n^1 (x_{\max}) - b\sqrt{u_n^1 (x_{\max})} \geq \varepsilon u_n^1 (x_{\max}).$$

Choosing $\varepsilon = 1/2$, from (8.36) we get (8.33). The argument for u_p^1 is similar. □

8.4. Further estimates for u^1, u_n^1, u_p^1

To proceed further we need to complete the control from below of u^1 and to verify that u_n^1, u_p^1 are bouded above by N. We replace in all the previous estimates the quantity M with the parameter M^* defined as

$$M^* = \frac{C_I C_L}{\min\left\{\varepsilon_j, C_m^0, C_m\right\}} (M_1^* + M_2^* + K_3)$$

with:

$$M_1^* = C_m^0 |\psi_N| + \lambda^{-2}\gamma_1 \|\rho\|_{L^2(\Omega_{1,3})} + \lambda^{-2}\gamma_2 \|\rho\|_{L^2(\Omega_2)} + \lambda^{-2}\gamma_1 \sum_{\alpha \neq o_2^-} \max\{u_{\alpha,N}, \bar{u}_\alpha\}, \tag{8.37a}$$

$$M_2^* = 2\lambda^{-2}\gamma_2 (R_2 - R_1) N. \tag{8.37b}$$

We also let:

$$U_{np}^* = \frac{e^{M^*}}{\min\left\{D_n, D_p\right\}} \left(\eta G + \frac{1}{\tau_p + \tau_n}\right), \tag{8.37c}$$

$$U_* = C^{EQ} e^{M^*} \left[\frac{k_n e^{M^*}}{k_1 \tilde{C}} N + 1\right], \tag{8.37d}$$

$$U_*' = D^{-1} e^{M^*} k_1 \tilde{C}. \tag{8.37e}$$

Lemma 8.10. *Assume that $u_\alpha^{(0)}, u^{(0)}, u_p^{(0)}, u_n^{(0)} \in \mathbf{X}$ (defined in (5.11)) and that $u^1 \geq \min\{u(R_1), u(R_2)\}$ in $\Omega_{1,3}$. Then, there exists $m > 0$, depending only on U_*, U_{np}^* and $\max\{u_{\alpha,N}, \bar{u}_\alpha\}$, such that*

$$\min\left\{u^1 (R_1), u^1 (R_2)\right\} \geq m. \tag{8.38}$$

Proof. Assume that there exists a sequence $u_j = \left\{(u_\alpha^{(0)}, u^{(0)}, u_p^{(0)}, u_n^{(0)})_j\right\} \in \mathbf{X}$ such that, say, $u_j(R_1) \to 0$. Same argument if $u_j(R_2) \to 0$. Correspondingly, there is a sequence of electric potentials $\left\{\psi_j\right\}$ equibounded in V.

Therefore there are sequences $\psi_{j_k}, u_{j_k}^{(1)}, \left(u_n^{(0)}\right)_{j_k}, \left(u_p^{(0)}\right)_{j_k}$ weakly convergent in their Sobolev spaces and strongly in C^* (by the compact embeddings of these spaces into C^*) to ψ^*, u^*, u_n^*, u_p^*. In particular, in Ω_1, u^* is a solution of the Robin-Neumann problem

$$-\frac{\partial}{\partial x}\left(De^{\psi^*}\frac{\partial u^*}{\partial x}\right) + \frac{k_1\tilde{C}\, e^{-\psi^*}}{C^{EQ}}u^* = k_1\tilde{C} \quad \text{in } \Omega_1$$

with $(u^*)'(0) = 0$ and

$$-De^{\psi^*\left(R_1^-\right)}(u^*)'\left(R_1^-\right) + k_p e^{\left[\psi^*\left(R_1^-\right)-\psi^*\left(R_1^+\right)\right]}u_p^*\left(R_1^+\right)u^*\left(R_1^-\right) = k_n e^{\psi^*\left(R_1^+\right)}u_n^*\left(R_1^+\right)e^{-g\left(\psi^*\left(R_1^-\right),u^*\left(R_1^-\right)\right)}.$$

However, we have also $u^*\left(R_1^-\right) = 0$ and $(u^*)'\left(R_1^-\right) = 0$, which imply $u^* \equiv 0$ in Ω_1. Contradiction. □

Lemma 8.11. *Let $u^0 \geq m^* = \min\left\{C^{EQ}e^{-M^*}, m\right\}$. If*

$$R_2 - R_1 \leq \frac{1}{2}\frac{1}{\sqrt{\min\left\{D_n, D_p\right\}e^{M^*}\left(\eta G + \left(\tau_p + \tau_n\right)^{-1}\right)}}. \tag{8.39a}$$

Then, we have

$$u_n \leq \max\{1, K_n\} \equiv K_n^*, \tag{8.39b}$$

$$u_p \leq \max\left\{1, K_p\right\} \equiv K_p^*, \tag{8.39c}$$

where:

$$K_n = 2(R_2 - R_1)\frac{n_i}{n_r k_n}e^{(M^*+|A|-\ln m^*)^2}\left(\eta G + \frac{1}{\tau_p + \tau_n}\right) \tag{8.39d}$$

$$K_p = 2(R_2 - R_1)\frac{n_i}{n_r k_p}\frac{e^{M^*}}{m^*}\left(\eta G + \frac{1}{\tau_p + \tau_n}\right). \tag{8.39e}$$

If we also assume that $R_2 - R_1$ is small enough to have (8.39a) and $K_n, K_p \leq N$, then from (8.18) we also have

$$\int_{\Omega_{1,3}} u \leq C^{EQ}e^{M^*}\left\{\frac{k_n e^{M^*}N}{k_1\tilde{C}} + 1\right\}. \tag{8.39f}$$

Proof. We start with the estimate for u_n. From $u^0 \geq m^*$, since $C^{EQ}e^{-M^*} < \tilde{C} < 1$, it follows that

$$g\left(\psi(R_1^-), u^{(0)}(R_1^-)\right),\ g\left(\psi(R_2^+), u^{(0)}(R_2^+)\right) \leq (|A| + M^* - \ln m^*)^2,$$

and from the weak formulation for u_n with $\varphi = 1$ we get

$$u_n\left(R_2^-\right), u_n\left(R_1^+\right) \leq (R_2 - R_1)\frac{n_i}{n_r}k_n e^{M^*+(|A|+M-\ln C^{EQ})^2}\left(\eta G + \frac{1}{\tau_p + \tau_n}\right).$$

Hence, using (8.30), we obtain

$$u_n(x_{\max}) = \int_{R_1}^{x_{\max}} u_n' + u_n(R_1^+) \leq (R_2 - R_1)\ \sqrt{D_n} e^{M^*/2} \sqrt{\eta G + \frac{1}{\tau_p + \tau_n}}\ \sqrt{u_n(x_{\max})} + u_n(R_1^+).$$

We distinguish two cases: either $u_n(x_{\max}) \leq 1$ or $u_n(x_{\max}) > 1$. In the latter case $\sqrt{u_n(x_{\max})} \leq u_n(x_{\max})$ and we can write

$$\left[1 - (R_2 - R_1)\ \sqrt{D_n} e^{M^*/2} \sqrt{\eta G + \frac{1}{\tau_p + \tau_n}}\right] u_n(x_{\max}) \leq u_n(R_1^+).$$

If (8.39a) holds, we deduce

$$u_n(x_{\max}) \leq 2(R_2 - R_1) \frac{n_i}{n_r k_n} e^{M + (|A| + 2M^* - \ln C^{EQ})^2} \left(\eta G + \frac{1}{\tau_p + \tau_n}\right)$$

We now address the estimate for u_p. From $u^0 \geq m^*$ and from the weak formulation for u_n with $\varphi = 1$ we get

$$u_p(R_2^-), u_p(R_1^+) \leq (R_2 - R_1) \frac{n_i}{n_r k_p} \frac{e^{M^*}}{m^*} \left(\eta G + \frac{1}{\tau_p + \tau_n}\right).$$

Hence, from (8.31), we have

$$u_p(x_{\max}) = \int_{R_1}^{x_{\max}} u_p' + u_p(R_1^+) \leq (R_2 - R_1)\ \sqrt{D_p} e^{M^*/2} \sqrt{\eta G + \frac{1}{\tau_p + \tau_n}}\ \sqrt{u_p(x_{\max})} + u_p(R_1^+).$$

From here on we can proceed as for u_n. □

8.5. Existence of a fixed point

We are now in the position to prove Theorem 5.1. The following assumptions are made:

Hp1 $\beta = \frac{C^{EQ} k_n}{k_1 \bar{C}} e^{M_1 + M_2}$ is sufficiently small according to Remark 8.2;

Hp2 $R_2 - R_1$ is sufficiently small to ensure that (8.32) and (8.34) are satisfied and that $K_2 \leq N$ and $K_p \leq N$.

Replace in all the estimates M with M^*, fix $(u_\alpha^{(0)}, u^{(0)}, u_p^{(0)}, u_n^{(0)}) \in \mathbf{X}$ and solve for $\psi^{(1)} = \mathcal{T}(u_\alpha^{(0)}, u^{(0)}, u_p^{(0)}, u_n^{(0)}) \in C^*$ (from Theorem 8.3). The map $\mathcal{T} : \mathbf{X} \to C^*$ is continuous and compact (from Theorem 8.4). Moreover, because of **Hp1** and **Hp2**, we have

$$\left\|\psi^{(1)}\right\|_{C^*}, \left\|\psi^{(1)}\right\|_V \leq M^*.$$

Given $\psi^{(1)}$, solve for $(u_\alpha^{(1)}, u^{(1)}, u_p^{(1)}, u_n^{(1)}) = \mathcal{P}(\psi^{(1)}, u_\alpha^{(0)}, u^{(0)}, u_p^{(0)}, u_n^{(0)})$. The map $\mathcal{P}$ is continuous and compact from $C^* \times \mathbf{X}$ into $\mathbf{X}$ (from Theorems 8.4, 8.5, 8.6 and 8.8). The application of Schauder Theorem concludes the proof of Theorem 5.1.

9. Conclusions and future perspectives

The continuous increase of questions regarding the coupling mechanisms in the bio-hybrid system constituted by a NP, a retinal neuron and the intermediate aqueous environment, has pushed the need for new tools to investigate the open problems in the realization of new generation retinal prostheses.

In our work we have proposed a mathematical model as a Virtual Laboratory complementing the indispensable experimental activity in the study and comprehension of the electrochemical phenomena that occur at the NP-neuron interface. In order to prove the reliability of our formulation, we have performed a theoretical study of the model, specifying the assumptions on the data that guarantee the existence of a solution to the nonlinear system of partial differential equations. Then, we have constructed a consistent and stable numerical approximation of the model based on the use of the finite element method. Finally, we have thouroughly investigated the numerical performance of the computational algorithm and the biophysical soundness of simulation predictions.

With the use of the proposed model we have been able to describe the coupled system comprising a neuron, an electrolytic solution and a NP immersed in the solution. We have taken into account the light-induced polarization of the NP as well as the interface photo-cathodic reaction of P3HT in an oxygenated environment. In particular, the choice of modeling the cleft as a fully electrolytic medium has revealed some limits of the model, wherein ions are able to totally screen the electrostatic charging of the NP. In the future, a better description of the proteinic nature of the cleft would help us provide a more faithful model picture of the electrostatic mechanisms which may occur at the bio-hybrid interface.

Regardless of the above mentioned limitations, the model has proved to be able to adequately represent the production and diffusion of O_2^- at the interface of the NP, thereby providing a quantitatively accurate estimate of the ROS molecule concentration in proximity of the neuron membrane as a function of the light intensity illuminating the NP.

Acknowledgements

Greta Chiaravalli and Guglielmo Lanzani were supported by the Italian Ministry of University and Research. Grant title: “Membrane targeted light driven nanoactuators for neuro-stimulation”; grant number: PRIN 2020XBFEMS.

Conflict of interest

The authors declare no conflict of interest.

References

1. E. Arnault, C. Barrau, C. Nanteau, P. Gondouin, K. Bigot, F. Viénot, et al., Phototoxic action spectrum on a retinal pigment epithelium model of age-related macular degeneration exposed to sunlight normalized conditions, *PLoS ONE*, **8** (2013), e71398. https://doi.org/10.1371/journal.pone.0071398
2. F. Benfenati, G. Lanzani, New technologies for developing second generation retinal prostheses, *Lab Anim.*, **47** (2018), 71–75. https://doi.org/10.1038/s41684-018-0003-1

3. S. Bellani, D. Fazzi, P. Bruno, E. Giussani, E. V. Canesi, G. Lanzani, et al., Reversible p3ht/oxygen charge transfer complex identification in thin films exposed to direct contact with water, *J. Phys. Chem. C*, **118** (2014), 6291–6299. https://doi.org/10.1021/jp4119309
4. G. Chiaravalli, G. Manfredi, R. Sacco, G. Lanzani, Photoelectrochemistry and drift-diffusion simulations in a polythiophene film interfaced with an electrolyte, *ACS Appl. Mater. Interfaces*, **13** (2021), 36595–36604. https://doi.org/10.1021/acsami.1c10158
5. H. Dember, Über eine photoelektronische kraft in kupferoxydul-kristallen, *Phys. Z.*, **32** (1931), 554.
6. S. Francia, D. Shmal, S. Di Marco, G. Chiaravalli, J. F. Maya-Vetencourt, G. Mantero, et al., Light-induced charge generation in polymeric nanoparticles restores vision in advanced-stage retinitis pigmentosa rats, *Nat. Commun.*, **13** (2022), 3677. https://doi.org/10.1038/s41467-022-31368-3
7. A. García-Layana, F. Cabrera-López, J. García-Arumí, L. Arias-Barquet, J. M. Ruiz-Moreno, Early and intermediate age-related macular degeneration: update and clinical review, *Clin. Interv. Aging*, **12** (2017), 1579–1587. https://doi.org/10.2147/CIA.S142685
8. D. Ghezzi, M. R. Antognazza, R. Maccarone, S. Bellani, E. Lanzarini, N. Martino, et al., A polymer optoelectronic interface restores light sensitivity in blind rat retinas, *Nature Photon.*, **7** (2013), 400–406. https://doi.org/10.1038/nphoton.2013.34
9. S. R. Goldman, K. Kalikstein, B. Kramer, Dember-effect theory, *J. Appl. Phys.*, **49** (1978), 2849–2854. https://doi.org/10.1063/1.325166
10. H. K. Gummel, A self-consistent iterative scheme for one-dimensional steady state transistor calculations, *IEEE Trans. Electron Dev.*, **11** (1964), 455–465. https://doi.org/10.1109/T-ED.1964.15364
11. F. G. Holz, S. Schmitz-Valckenberg, M. Fleckenstein, Recent developments in the treatment of age-related macular degeneration, *J. Clin. Invest.*, **124** (2014), 1430–1438. https://doi.org/10.1172/JCI71029
12. J. W. Jerome, *Analysis of charge transport*, Heidelberg: Springer, 1996. https://doi.org/10.1007/978-3-642-79987-7
13. J. W. Jerome, Analytical approaches to charge transport in a moving medium, *Transport Theory Stat. Phys.*, **31** (2002), 333–366. https://doi.org/10.1081/TT-120015505
14. J. W. Jerome, R. Sacco, Global weak solutions for an incompressible charged fluid with multi-scale couplings: initial–boundary-value problem, *Nonlinear Anal.*, **71** (2009), e2487–e2497. https://doi.org/10.1016/j.na.2009.05.047
15. J. Q. Li, T. Welchowski, M. Schmid, M. M. Mauschitz, F. G. Holz, R. P. Finger, Prevalence and incidence of age-related macular degeneration in Europe: a systematic review and meta-analysis, *Brit. J. Ophthalmol.*, **104** (2020), 1077–1084. https://doi.org/0.1136/bjophthalmol-2019-314422
16. J. L. Lions, E. Magenes, *Non-homogeneous boundary value problems and applications (Vol. 1)*, Heidelberg: Springer, 1972. https://doi.org/10.1007/978-3-642-65161-8
17. R. A. Marcus, On the theory of electron-transfer reactions. VI. Unified treatment for homogeneous and electrode reactions, *J. Chem. Phys.*, **43** (1965), 679. https://doi.org/10.1063/1.1696792
18. P. A. Markowich, *The stationary semiconductor device equations*, Vienna: Springer, 1986. https://doi.org/10.1007/978-3-7091-3678-2

19. N. L. Mata, R. Vogel, Pharmacologic treatment of atrophic age-related macular degeneration, *Curr. Opin. Ophthalmol.*, **21** (2010), 190–196. https://doi.org/10.1097/ICU.0b013e32833866c8
20. J. F. Maya-Vetencourt, G. Manfredi, M. Mete, E. Colombo, M. Bramini, S. Di Marco, et al., Subretinally injected semiconducting polymer nanoparticles rescue vision in a rat model of retinal dystrophy, *Nat. Nanotechnol.*, **15** (2020), 698–708. https://doi.org/10.1038/s41565-020-0696-3
21. K. L. Pennington, M. M. DeAngelis, Epidemiology of age-related macular degeneration (AMD): associations with cardiovascular disease phenotypes and lipid factors, *Eye Vision*, **3** (2016), 1–20. https://doi.org/10.1186/s40662-016-0063-5
22. S. Picaud, J.-A. Sahel, Retinal prostheses: clinical results and future challenges, *C. R. Biol.*, **337** (2014). 214–222. https://doi.org/10.1016/j.crvi.2014.01.001
23. I. Rubinstein, *Electro-diffusion of ions*, SIAM, 1990. https://doi.org/10.1137/1.9781611970814
24. R. Sacco, G. Guidoboni, A. G. Mauri, *A comprehensive physically based approach to modeling in bioengineering and life sciences*, Academic Press, 2019. https://doi.org/10.1016/C2016-0-02357-4
25. D. L. Scharfetter, H. K. Gummel, Large-signal analysis of a silicon Read diode oscillator, *IEEE Trans. Electron Dev.*, **16** (1969), 64–77. https://doi.org/10.1109/T-ED.1969.16566
26. U. Schmidt-Erfurth, T. Hasan, Mechanisms of action of photodynamic therapy with verteporfin for the treatment of age-related macular degeneration, *Surv. Ophthalmol.*, **45** (2000), 195–214. https://doi.org/10.1016/S0039-6257(00)00158-2
27. M. Schmuck, Analysis of the Navier-Stokes-Nernst-Planck-Poisson system, *Math. Mod. Meth. Appl. Sci.*, **19** (2009), 993–1014. https://doi.org/10.1142/S0218202509003693
28. W. Shockley, W. T. Read, Statistics of the recombinations of holes and electrons, *Phys. Rev.*, **87** (1952), 835–842. https://doi.org/10.1103/PhysRev.87.835
29. J. W. Slotboom, Computer-aided two-dimensional analysis of bipolar transistors, *IEEE Trans. Electron Dev.*, **20** (1973), 669–679. https://doi.org/10.1109/T-ED.1973.17727
30. W. Van Roosbroeck, Theory of flow of electrons and holes in germanium and other semiconductors, *The Bell System Technical Journal*, **29** (1950), 560–607. https://doi.org/10.1002/j.1538-7305.1950.tb03653.x
31. A. L. Wang, D. K. Knight, T.-T. T. Vu, M. C. Mehta, Retinitis pigmentosa: review of current treatment, *International Ophthalmology Clinics*, **59** (2019), 263–280. https://doi.org/10.1097/IIO.0000000000000256
32. J. O. Winter, S. F. Cogan, J. F. Rizzo, Retinal prostheses: current challenges and future outlook, *J. Biomat. Sci. Polym. Ed.*, **18** (2007), 1031–1055. https://doi.org/10.1163/156856207781494403

AIMS Press